Diversity and Evolution of Mineralized Skeletal Tissues in Chondrichthyans

Fidji Berio [1,2]*, Morgane Broyon [3,4], Sébastien Enault [1], Nelly Pirot [3,4], Faviel A. López-Romero [5] and Mélanie Debiais-Thibaud [1]*

[1] ISEM, CNRS, EPHE, IRD, Univ. Montpellier, Montpellier, France, [2] University of Lyon, ENS Lyon, CNRS, Université Claude Bernard Lyon 1, Institut de Génomique Fonctionnelle de Lyon, UMR 5242, Lyon, France, [3] BCM, CNRS, INSERM, Univ. Montpellier, Montpellier, France, [4] IRCM, ICM, INSERM, Univ. Montpellier, Montpellier, France, [5] Department of Palaeontology, University of Vienna, Vienna, Austria

The diversity of skeletal tissues in extant vertebrates includes mineralized and unmineralized structures made of bone, cartilage, or tissues of intermediate nature. This variability, together with the diverse nature of skeletal tissues in fossil species question the origin of skeletonization in early vertebrates. In particular, the study of skeletal tissues in cartilaginous fishes is currently mostly restrained to tessellated cartilage, a derived form of mineralized cartilage that evolved at the origin of this group. In this work, we describe the architectural and histological diversity of neural arch mineralization in cartilaginous fishes. The observed variations in the architecture include tessellated cartilage, with or without more massive sites of mineralization, and continuously mineralized neural arches devoid of tesserae. The histology of these various architectures always includes globular mineralization that takes place in the cartilaginous matrix. In many instances, the mineralized structures also include a fibrous component that seems to emerge from the perichondrium and they may display intermediate features, ranging from partly cartilaginous to mostly fibrous matrix, similar to fibrocartilage. Among these perichondrial mineralized tissues is also found, in few species, a lamellar arrangement of the mineralized extracellular matrix. The evolution of the mineralized tissues in cartilaginous fishes is discussed in light of current knowledge of their phylogenetic relationships.

Keywords: cartilaginous fishes (chondrichthyes), gnathostomes, lamellar mineralization, neural arches, perichondrium, tesserae

1. INTRODUCTION

The classical view in vertebrate skeletal biology is mainly driven by the extensive work made in tetrapod species, in which clear distinctions are made between several cartilaginous and bony tissues (Hall, 2015). According to this classical view, cartilaginous tissues are retained in only a few sites in the adult skeleton and are classified into hyaline, elastic, and fibro-cartilages that display various assemblages of collagen fibers (Wachsmuth et al., 2006). Hyaline cartilage appears as a transparent tissue whose extracellular matrix does not display histologically observable fibers. The extracellular matrix of hyaline cartilage is characterized by type II collagen running through high contents of proteoglycans with acidic glycosaminoglycans that sequestrate water (Hall, 2015). Bone is defined by the deposition of type I collagen-rich extracellular matrix with little to no acidic glycosaminoglycans deposited, which undergoes mineralization through the activity of osteocytes (Hall, 2015).

Molecular and paleontological evidence has allowed the elaboration of a timeframe for the emergence of the various vertebrate skeletal tissues. Hyaline cartilage is ancestral to vertebrates (Zhang and Cohn, 2006) and most probably evolved earlier than vertebrates (Tarazona et al., 2016), while dermal and perichondrial bone, but also globular mineralized cartilage, is found in early agnathan vertebrates (Donoghue and Sansom, 2002). Among jawed vertebrates, the skeleton of extant cartilaginous fishes (chondrichthyans) is considered to be made exclusively of cartilage, with different types of mineralization that were described in early classical works (Hasse, 1879; Ridewood and MacBride, 1921; Ørvig, 1951; Applegate, 1967). Cartilage mineralization in chondrichthyans mainly occurs under the form of tesserae that are small articulated units of cartilage impregnated with apatite and are a shared derived character of this group (reviewed in Maisey et al., 2020). Paleontological evidence, therefore, implies that cartilaginous fishes have lost dermal and perichondrial bone more than 400 million years ago (Donoghue and Sansom, 2002). Several genetic data were interpreted in light of this evolutionary framework for skeletal tissues, however, our knowledge of chondrichthyan genomes remains scarce (Ryll et al., 2014; Enault et al., 2015; Debiais-Thibaud et al., 2019; Leurs et al., 2021).

More recent studies have reassessed the diversity of poorly described features of mineralization in cartilaginous fishes (Eames et al., 2007; Enault et al., 2015; Seidel et al., 2017, 2020; Atake et al., 2019; Debiais-Thibaud, 2019; Smith et al., 2019; Chaumel et al., 2020; Pears et al., 2020), raising new questions on the origin and evolution of mineralized tissues in this clade and therefore in vertebrates. Comparative studies of skeletal tissues in non-tetrapods have uncovered a wide range of skeletal tissues that had remained unknown from the sole study of tetrapods (discussed by Witten and Huysseune, 2009 and Hall and Witten, 2019). Teleost fishes display for example a wide variety of skeletal tissues with intermediate features (e.g., hyaline, elastic, fibrous, whether mineralized or not) of what is classically associated to either bone or cartilage and for which standard characterization by histology has been proposed (Witten et al., 2010; Hall and Witten, 2019). A wider description of the diversity of skeletal tissues in non-tetrapod species is therefore still needed to understand the origin and the diversification of mineralized tissues in vertebrates. In this study, we chose to focus on the comparative analysis of mineralized cartilage in the neural arches of chondrichthyans.

Extant chondrichthyans include three major clades. Holocephalans are divided into the three extant families Callorhinchidae, Chimaeridae, and Rhinochimaeridae and have long been considered to have a non-mineralized cartilaginous endoskeleton but are now recognized to have tesserae (Finarelli and Coates, 2014; Maisey et al., 2020; Pears et al., 2020; Seidel et al., 2020). Sister to holocephalans, elasmobranchs include selachians (sharks) that are grouped into Galeomorphii (orders: Carcharhiniformes, Heterodontiformes, Lamniformes, and Orectolobiformes) and Squalomorphii (orders: Hexanchiformes, Pristiophoriformes, Squaliformes, Squatiniformes, and the family Echinorhinidae) and batoids (rays, guitarfishes, skates, and sawfishes) that are divided into Myliobatiformes,

Rhinopristiformes, Rajiformes, and Torpediniformes (Naylor et al., 2012; Ebert et al., 2013; Last et al., 2016). Most cartilaginous endoskeletal elements of selachians and batoids are covered by tesserae (e.g., the jaws, fins, and most vertebral elements) (Dean et al., 2009; Chaumel et al., 2020). The tesseral body (the internal part of a tessera) contains type II collagen, round cells enclosed in lacunae, and Liesegang lines typical of globular mineralization (Kemp and Westrin, 1979; Seidel et al., 2017; Chaumel et al., 2020). The tesseral cap zone (the external part of a tessera) is located on the perichondrial side and is characterized by flatter cells engulfed in a type I collagen matrix (Ørvig, 1951; Kemp and Westrin, 1979; Seidel et al., 2017; Chaumel et al., 2020). This cap zone has been discussed as a remnant, or derived version of an ancestral bony tissue in jawed vertebrates (Kemp and Westrin, 1979; Seidel et al., 2017).

Less studied than tesserae are two other mineralized tissues, also reported in the elasmobranch endoskeleton by Ørvig (1951), and reviewed by Dean and Summers (2006) and Debiais-Thibaud (2019). On the one hand, areolar mineralization characterizes the vertebral centra of elasmobranchs (Ridewood and MacBride, 1921). On the other hand, a type of lamellar mineralization has been identified only in the vertebral neural arches and repeatedly compared to bone tissue (Peignoux-Deville et al., 1982; Eames et al., 2007; Atake et al., 2019). Until now, this lamellar mineralization, or bone-like tissue, was reported in two shark species within Carcharhiniformes [the small-spotted catshark *Scyliorhinus canicula* (Peignoux-Deville et al., 1982) and the swellshark *Cephaloscyllium ventriosum* (Eames et al., 2007)], and in two batoid species belonging to Rajiformes [the Eaton's skate *Bathyraja eatonii* and the little skate *Leucoraja erinacea* (Atake et al., 2019)]. The similarity between lamellar mineralization and bone tissue was raised several times—it was first termed osseous tissue by Peignoux-Deville et al. (1982)— because of the occurrence of elongated cells similar to osteoblasts in bone (Peignoux-Deville et al., 1982) that express type I collagen genes (Enault et al., 2015) and because these cells are enclosed in a type I collagen-rich extracellular matrix, which is able to mineralize (Eames et al., 2007). This type of mineralization differs from the classical globular mineralization described in the cartilage of fossils (Ørvig, 1951) and the body zone of tesserae (Kemp and Westrin, 1979; Seidel et al., 2017).

In this study, we first provide microCT images to visualize the architecture of mineralized tissues in the neural arches in ten orders of elasmobranchs and one holocephalan family. We then use classical histology to illustrate cell shape and extracellular matrix characteristics (e.g., fibrous or hyaline nature, presence of acidic proteoglycans) to describe the mineralized tissues. The results provide insights into the evolutionary history of endoskeletal mineralization among chondrichthyans and question the nature of the mineralized tissues described in early gnathostomes and vertebrates.

2. MATERIALS AND METHODS

2.1. Biological Sampling

The dataset includes 19 specimens from 16 species of chondrichthyans (**Table 1**) and covers six of the eight orders

TABLE 1 | Chondrichthyan samples used for histology and microCT scanning.

Subclass	Superorder	Order	Family	Species	Growth stage	Fixation	Decalcification	Section
Elasmobranchii	Galeomorphii	Heterodontiformes	Heterodontidae	*Heterodontus francisci*	Subadult (Meese and Lowe, 2020)	80% ethanol	Yes	posterior
Elasmobranchii	Galeomorphii	Orectolobiformes	Hemiscyllidae	*Chiloscyllium punctatum*	Juvenile (Compagno, 1984)	4% PFA	No	anterior
Elasmobranchii	Galeomorphii	Lamniformes	Odontaspididae	*Carcharias taurus*	Sexually mature (Lucifora et al., 2002)	4% PFA	Yes	anterior
Elasmobranchii	Galeomorphii	Carcharhiniformes	Triakidae	*Galeorhinus galeus*	Juvenile (Lucifora et al., 2004)	80% ethanol	Yes	anterior
Elasmobranchii	Galeomorphii	Carcharhiniformes	Carcharhinidae	*Prionace glauca*	Juvenile (Bustamante and Bennett, 2013)	100% ethanol	Yes	posterior
Elasmobranchii	Galeomorphii	Carcharhiniformes	Scyliorhinidae	*Scyliorhinus canicula*	Embryo (Enault et al., 2016)	4% PFA	No	anterior
Elasmobranchii	Galeomorphii	Carcharhiniformes	Scyliorhinidae	*Scyliorhinus canicula*	Juvenile (Capapé et al., 2008)	4% PFA	No	anterior
Elasmobranchii	Galeomorphii	Carcharhiniformes	Sphyrnidae	*Sphyrna lewini*	Juvenile (Bejarano-Álvarez et al., 2011)	80% ethanol	Yes	posterior
Elasmobranchii	Squalomorphii	Squaliformes	Somniosidae	*Centroscymnus crepidater**	Juvenile (Moore et al., 2013)	70% ethanol	No	posterior
Elasmobranchii	Squalomorphii	Squaliformes	Etmopteridae	*Etmopterus spinax**	Juvenile (Porcu et al., 2014)	70% ethanol	No	posterior
Elasmobranchii	Squalomorphii	Squatiniformes	Squatinidae	*Squatina californica*	Sexually mature (Romero-Caicedo et al., 2016)	80% ethanol	Yes	posterior
Elasmobranchii	Batoidea	Myliobatiformes	Gymnuridae	*Gymnura micrura**	Sexually mature (Yokota et al., 2012)	70% ethanol	Yes	posterior
Elasmobranchii	Batoidea	Rhinopristiformes	Rhinobatidae	*Pseudobatos productus*	Sexually mature (Márquez-Farías, 2007)	80% ethanol	Yes	posterior
Elasmobranchii	Batoidea	Rhinopristiformes	Rhinidae	*Rhina ancylostoma*	147 cm TL	4% PFA	Yes	posterior
Elasmobranchii	Batoidea	Torpediniformes	Torpedinidae	*Torpedo* sp.*	16 cm DW	70% ethanol	Yes	posterior
Elasmobranchii	Batoidea	Rajiformes	Rajidae	*Raja clavata*	Hatchling	4% PFA	No	ant, posterior
Elasmobranchii	Batoidea	Rajiformes	Rajidae	*Raja clavata*	Juvenile (Capapé et al., 2007)	70% ethanol	No	posterior
Holocephali	–	Chimaeriformes	Chimaeridae	*Hydrolagus colliei*	Hatchling	100% ethanol	No	anterior (sy)
Holocephali	–	Chimaeriformes	Chimaeridae	*Hydrolagus colliei**	Juvenile (Barnett et al., 2009)	70% ethanol	No	anterior (sy)

DW, disc width; PFA, paraformaldehyde; sy, synarcual; TL, total length. When no literature data are available on the size at sexual maturity for a species, the TL or DW are indicated. Asterisks indicate the specimens that have been preserved in ethanol for several decades.

of extant sharks, the four orders of extant batoids, and one of the three families of extant Chimaeriformes (Naylor et al., 2012; Ebert et al., 2013; Last et al., 2016). The samples were kindly provided by the University of Montpellier, by the Aquarium of Montpellier (Planet Ocean Montpellier), or were bought at fish markets. No handling of live specimens was necessary for this study. The ontogenetic stages were determined based on literature data, using the total length (TL) or disc width (DW) as proxies (**Table 1**). When no data were available about the ontogenetic stages of the species sampled, the TL, DW, or both were provided (**Table 1**). When fresh or frozen material was available, the vertebra or neural arch were sampled and fixed in 4% paraformaldehyde in Phosphate-Buffered Saline 1X (PBS 1X). Anterior and posterior vertebrae were sampled anterior and posterior to the pelvic girdle, respectively. Samples made from long-term stored material were first rinsed in fresh ethanol for 48 h before further processing (note that some specimens come from collections in ethanol that date back from the 90's, see details in **Table 1**).

2.2. Histological Staining

Alizarin Red S staining on thick (circa 1 mm) slices was performed overnight in a potassium hydroxide (KOH) 0.5% solution with a concentration of Alizarin Red S of 0.005% for samples of *S. canicula* and the thornback ray *Raja clavata*, or 0.05% for samples of the spotted ratfish *Hydrolagus colliei*. Stained samples were progressively equilibrated in 25% glycerol in KOH 0.5%, 50% glycerol in KOH 0.5%, 75% glycerol in KOH 0.5%, and glycerol 100% before being imaged under a binocular (Leica Microsystems). Only samples fixed in paraformaldehyde were used for this staining procedure.

A double Alizarin Red S and Alcian Blue staining was performed on a 14 μm-thick cryostat section made in a non-demineralized portion of the anterior vertebral column of an embryonic lesser spotted catshark fixed in 4% PFA. The section was rinsed in PBS 1X, then in KOH 0.5% before a bath of Alizarin Red S 0.005% in KOH 0.5% for 1 min. The slide was rinsed once in PBS 1X, incubated for 2 min in a 0.02% Alcian blue 8G solution (8:2 ethanol/glacial acetic acid), washed once in EtOH 100%, and once in PBS 1X before being mounted in Mowiol.

For other histological staining protocols, samples exhibiting strong vertebral mineralization were first rehydrated and then demineralized with Thermo Scientific Shandon TBD-2 decalcifier during 24–48 h before the embedding process (**Table 1**). Samples were progressively dehydrated in 70, 96, and 100% ethanol before paraffin embedding. Paraffin-embedded tissue was cut into 7 μm-thick sections, mounted on slides in an alternate consecutive fashion, and dried at 37 °C overnight. Tissue sections were stained with Hematoxylin, Eosin, and Saffron with HMS 740 autostainer (MM France) for preliminary analysis. The Hematoxylin-Eosin-Saffron (HES) protocol stains basophilic components in deep violet [nuclei and basophilic extracellular matrices (H)], cytoplasm in pink (E), and collagen fibers in bright orange (S), allowing a fine description of cell and matrix morphologies. HES has poor staining contrast on hyaline cartilage (gray or beige uniform staining) but allows contrasting the cartilaginous matrix with perichondral tissue because of the

eosinophilic and Saffron-positive staining of the fibrous matrix (Hilton et al., 2005). The modified cartilaginous extracellular matrix in cartilage mineralizing zones is also contrasted in HES (Mayoral et al., 2014), possibly because it is basophilic. Tissue sections were also stained with PAS-AB, which associates the standard Alcian blue method (AB, pH 2.5, standard staining for acid mucins in hyaline cartilage matrix, blue staining) with the Periodic Acid Schiff (PAS) technique to distinguish with neutral mucins (magenta staining). PAS-AB staining is a standard for the detection of hyaline cartilage matrix, as the staining is associated with the acidic glycosaminoglycan content of the matrix (Whiteman, 1973). Previous work has shown that Alcian blue stains best in the proliferative and resting chondrocyte zone of endochondral bone, while the PAS magenta stains both the fibrous perichondrium and the hypertrophic chondrocyte zones (Xiong et al., 2005). Some variation in the intensity and color of HES and PAS-AB assays between samples are observed, which most probably results from variations in the fixation, decalcification, and storage solutions, but also from an important variation in the storage time of our samples. Despite these variations, cell shape was still well-preserved and there was good correspondence between the locations of mineralization (as defined by microCT images) and the places of modified staining with HES in the cartilaginous and fibrous extracellular matrices. Mounted histological slides were scanned with a Hamamatsu NanoZoomer 2.0-HT scanner in the local MRI platform and images were visualized with the NDP.view software (v1.2.47).

2.3. Micro-Computed Tomography

Micro-computed tomography (microCT) was performed on selected vertebral samples preserved in alcohol with EasyTom 150 and reconstructed with the Xact software (v11025). The images were subsequently analyzed with the Avizo Lite software (v2019.3).
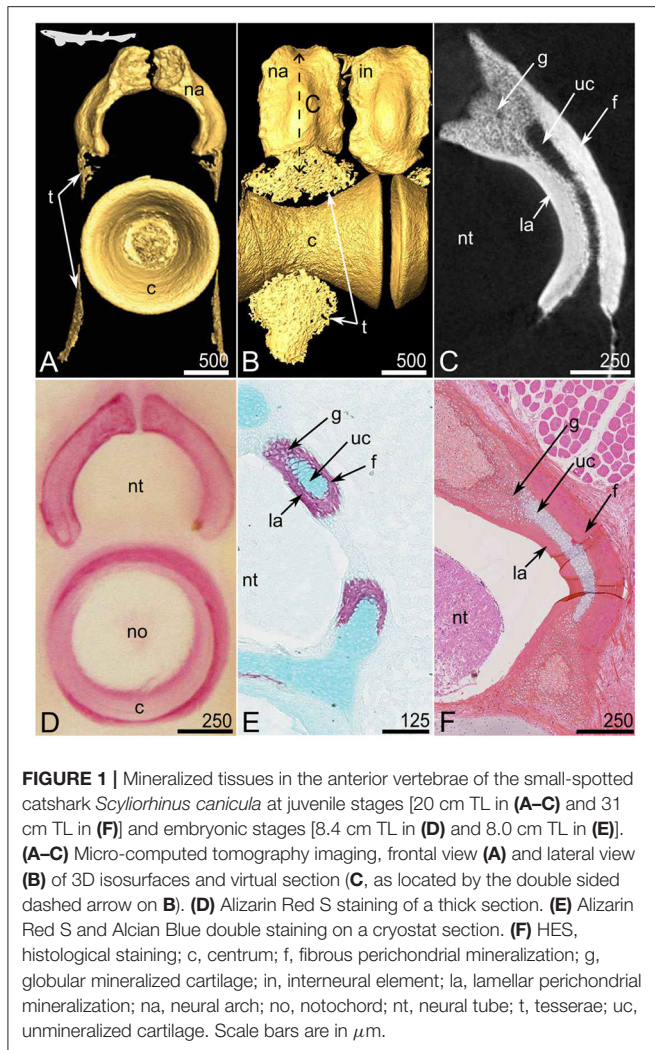
2.4. Ancestral Character State Reconstruction

For each character identified in our results, we built a character matrix and used phylogenetic relationships from Licht et al. (2012), Naylor et al. (2012), and Last et al. (2016). We reconstructed the ancestral state for each character (globular mineralization, fibrous mineralization, and lamellar mineralization: presence/absence; mineralization architecture: continuous/semi-discontinuous/discontinuous (tessellated or reduced) with Mesquite (v3.61) (Maddison and Maddison, 2019).

3. RESULTS

## 3.1. Anatomical and Histological Features of Neural Arches in Three Reference Species

We first selected reference species among the three main chondrichthyan clades: *S. canicula* (Carcharhiniformes, Galeomorphii) (**Figures 1**, **2**), *R. clavata* (Rajiformes, Batoidea) (**Figure 3**), and *H. colliei* (Chimaeriformes, Holocephali)

FIGURE 1 | Mineralized tissues in the anterior vertebrae of the small-spotted catshark *Scyliorhinus canicula* at juvenile stages [20 cm TL in **(A–C)** and 31 cm TL in **(F)**] and embryonic stages [8.4 cm TL in **(D)** and 8.0 cm TL in **(E)**]. **(A–C)** Micro-computed tomography imaging, frontal view **(A)** and lateral view **(B)** of 3D isosurfaces and virtual section (**C**, as located by the double sided dashed arrow on **B**). **(D)** Alizarin Red S staining of a thick section. **(E)** Alizarin Red S and Alcian Blue double staining on a cryostat section. **(F)** HES, histological staining; c, centrum; f, fibrous perichondrial mineralization; g, globular mineralized cartilage; in, interneural element; la, lamellar perichondrial mineralization; na, neural arch; no, notochord; nt, neural tube; t, tesserae; uc, unmineralized cartilage. Scale bars are in μm.

FIGURE 2 | Histological characterization of the mineralized tissues in the anterior vertebrae of the small-spotted catshark *Scyliorhinus canicula* at an embryonic stage [7 cm TL in **(A,B)**] and a juvenile stage [31 cm TL in **(C,D)**]. Serial sections were stained with HES **(A,C)** and PAS-AB **(B,D)**. **(A',C')** Close-ups of the boxed zones in **(A,C)**, respectively. Close-up on the lamellar (la), globular (g), and fibrous (f) mineralized tissues: **(C1–C3,D1–D3)** are details of **(C',D)**, respectively. f, fibrous perichondrial mineralization; fib, fibrocyte-shaped cell; g, globular mineralized cartilage; hc, hyaline cartilage; la, lamellar perichondrial mineralization; lam, lamella; Li, Liesegang lines; m, muscle tissue; no, notochord; nt, neural tube; pc, perichondrium; ps, pericellular space; uc, unmineralized cartilage. Vertical lines in **(C',D)** delimit the fibrous and hyaline cartilaginous matrices. Dashed lines in **(C',D)** locate the zones of mineralized matrix. Black arrow points to fibrous extracellular matrix. Scale bars are in μm.

(**Figure 4**). The description of the vertebrae of these species is provided first because of their representativeness in the chondrichthyan phylogeny, also because literature data shows a strong variation in the type of mineralized tissues in their neural arches (Debiais-Thibaud, 2019), and because we had specimens of successive ontogenetic stages allowing developmental comparisons.

3.1.1. Neural Arch Mineralization in *Scyliorhinus canicula*

Each anterior (thoracic) vertebra of *S. canicula* includes a mineralized, hourglass-shaped, centrum (**Figures 1A,B**). Each centrum is dorsally overlaid by a mineralized neural arch that alternates with interneural elements, both (neural and interneural elements) appearing similar in shape but interneurals are located dorsal to the junction between two centra (**Figures 1A,B**). The vertebral body surface also shows thin zones of mineralization (lace-like mineralization, **Figures 1A,B**) that are small tesserae (see details below and in **Figure 5**). The neural arches and interneural elements externally appear
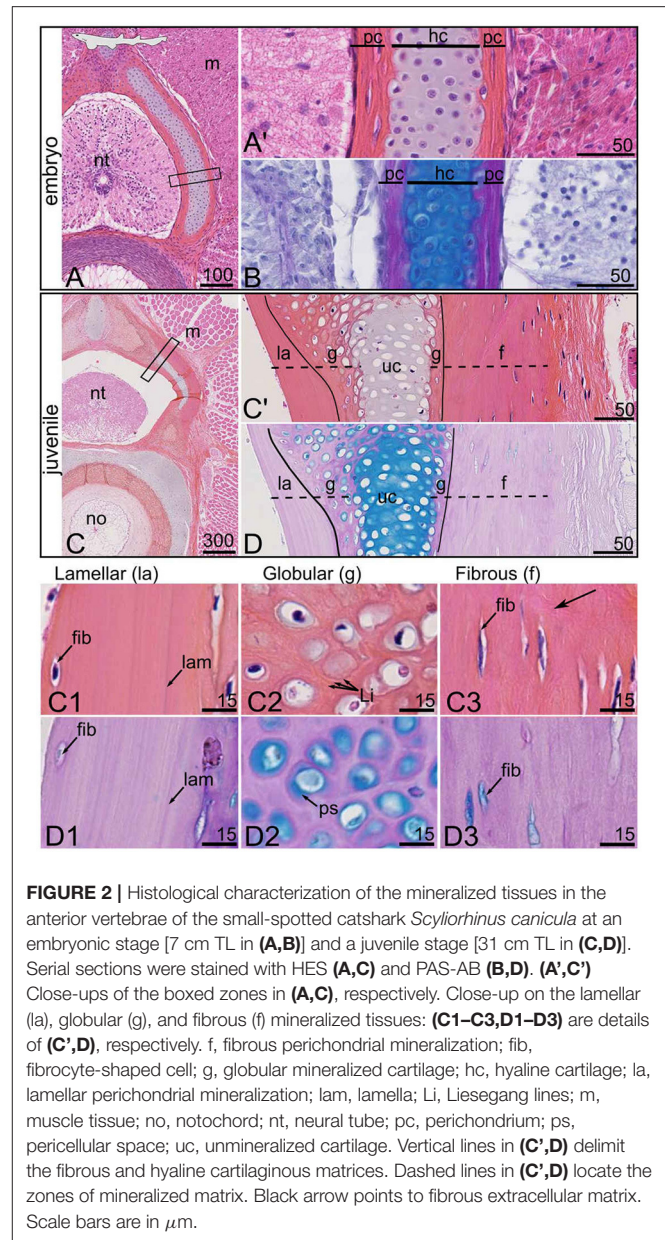
as continuously mineralized structures (**Figures 1A,B**) but the virtual (microCT) and histological sections reveal that the mineralized layer encloses an inner core of unmineralized tissue (**Figures 1C,E,F**) of cartilaginous nature (**Figures 1E,F**). In the following, we used HES and PAS-AB histological staining protocols to characterize cells and their extracellular matrix in each vertebral tissue. We previously successfully used HES staining to characterize cartilaginous matrix mineralization in chondrichthyans (Enault et al., 2015; Debiais-Thibaud, 2019). Mineralized zones (stained with Alizarin Red S in **Figure 1D**) appear dark pink in comparison to the unmineralized matrix (**Figure 1F**, compare g with uc zones), probably because of an eosinophilic nature. The comparison between the virtual and
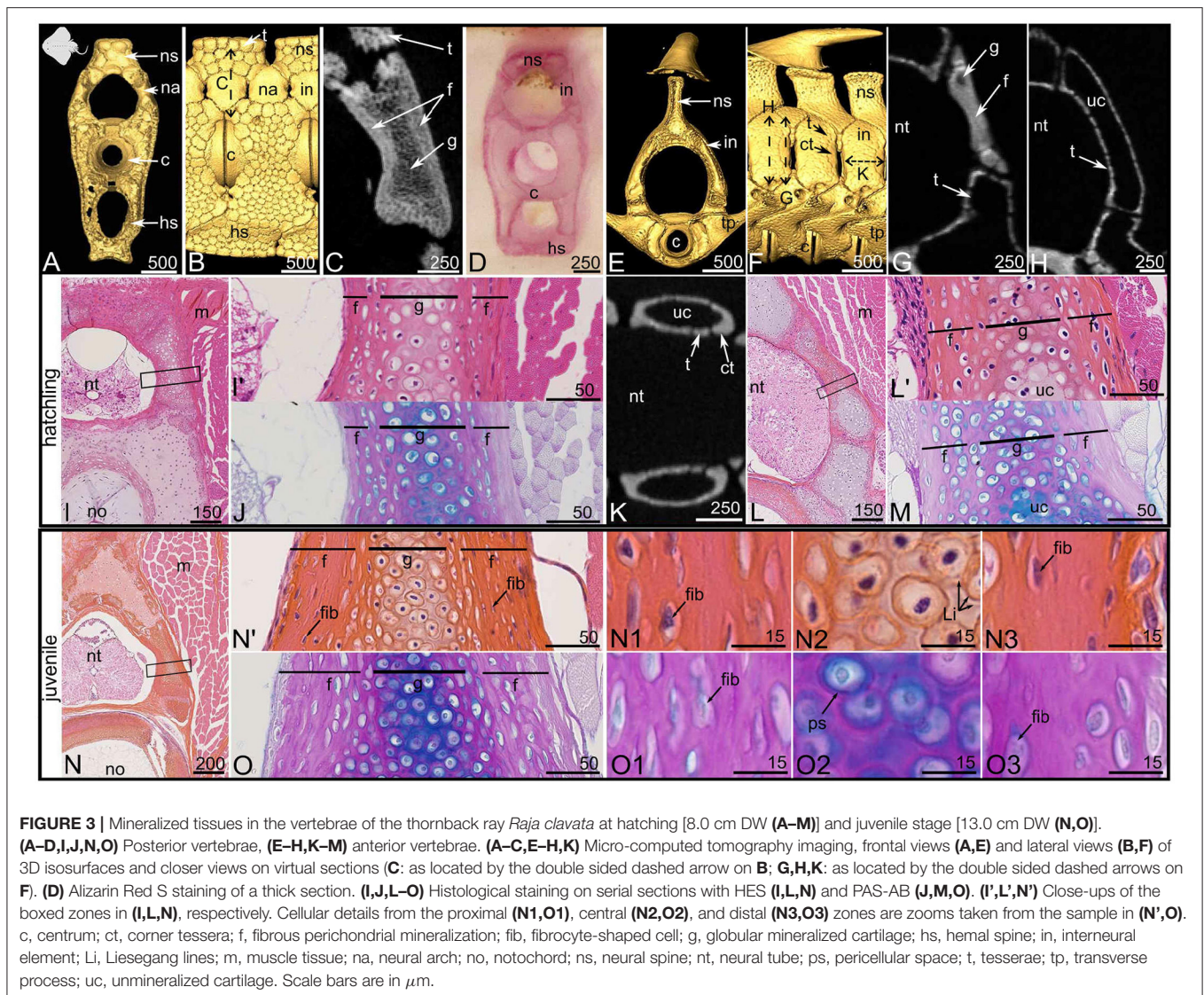
FIGURE 3 | Mineralized tissues in the vertebrae of the thornback ray *Raja clavata* at hatching [8.0 cm DW **(A–M)**] and juvenile stage [13.0 cm DW **(N,O)**].
(A–D,I,J,N,O) Posterior vertebrae, **(E–H,K–M)** anterior vertebrae. **(A–C,E–H,K)** Micro-computed tomography imaging, frontal views **(A,E)** and lateral views **(B,F)** of
3D isosurfaces and closer views on virtual sections **(C**: as located by the double sided dashed arrow on **B**; **G,H,K**: as located by the double sided dashed arrows on
F). **(D)** Alizarin Red S staining of a thick section. **(I,J,L–O)** Histological staining on serial sections with HES **(I,L,N)** and PAS-AB **(J,M,O)**. **(I',L',N')** Close-ups of the
boxed zones in **(I,L,N)**, respectively. Cellular details from the proximal **(N1,O1)**, central **(N2,O2)**, and distal **(N3,O3)** zones are zooms taken from the sample in **(N',O)**.
c, centrum; ct, corner tessera; f, fibrous perichondrial mineralization; fib, fibrocyte-shaped cell; g, globular mineralized cartilage; hs, hemal spine; in, interneural
element; Li, Liesegang lines; m, muscle tissue; na, neural arch; no, notochord; ns, neural spine; nt, neural tube; ps, pericellular space; t, tesserae; tp, transverse
process; uc, unmineralized cartilage. Scale bars are in μm.

histological sections (**Figures 1C,F**) allows identifying several
types of mineralized tissue. First, there is a zone displaying cell
spherical lacunae, where mineralization is less dense (lower gray
level in **Figure 1C**), and that is located in the dorsal-most zone
of the cartilaginous core (g in **Figure 1**). Denser mineralized
zones (deeper white in **Figure 1C**) cover the inner unmineralized
cartilage rod (uc in **Figure 1**). These perichondrial zones are
further differentiated in the proximal perichondrium (facing the
neural tube, la in **Figure 1**) and the distal perichondrium (facing
the thoracic muscles, f in **Figure 1**) through the HES and PAS-AB
staining protocols.

In the embryonic developing neural arches (**Figures 2A,B**),
at a stage when mineralization initiates (Enault et al., 2016), the
fibrous perichondrial tissue is characterized by flat cells enclosed
in a fibrous extracellular matrix (pc in **Figure 2A'**), while the
internal cartilaginous tissue stains positive for Alcian blue in
Figure 2B).

In the juvenile specimen in which structures are fully
mineralized, the neural arch is organized as a central,
unmineralized cartilaginous rod (uc in **Figures 2C',D**). This
internal cartilaginous rod is no more than 100 μm wide in
the juvenile specimen, which is similar to what is observed
in the hatchling specimen, suggesting that this internal
tissue does not significantly grow between these ontogenetic
stages (**Figures 2A,C**). In continuity with this cartilaginous
unmineralized rod, the most dorsal and ventral aspects appear
mineralized (**Figures 1C,E,F**, **2C',D**) together with the contact
surface with the perichondrium (g in **Figures 2C',D**). The
perichondrium is characterized by low to absent Alcian blue
staining in the PAS-AB assay (**Figure 2D**) and by elongated
cells engulfed in a Saffron stained extracellular matrix in the
HES assay (**Figure 2C'**). Several differences in cell density and
matrix organization can be detected when comparing the distal
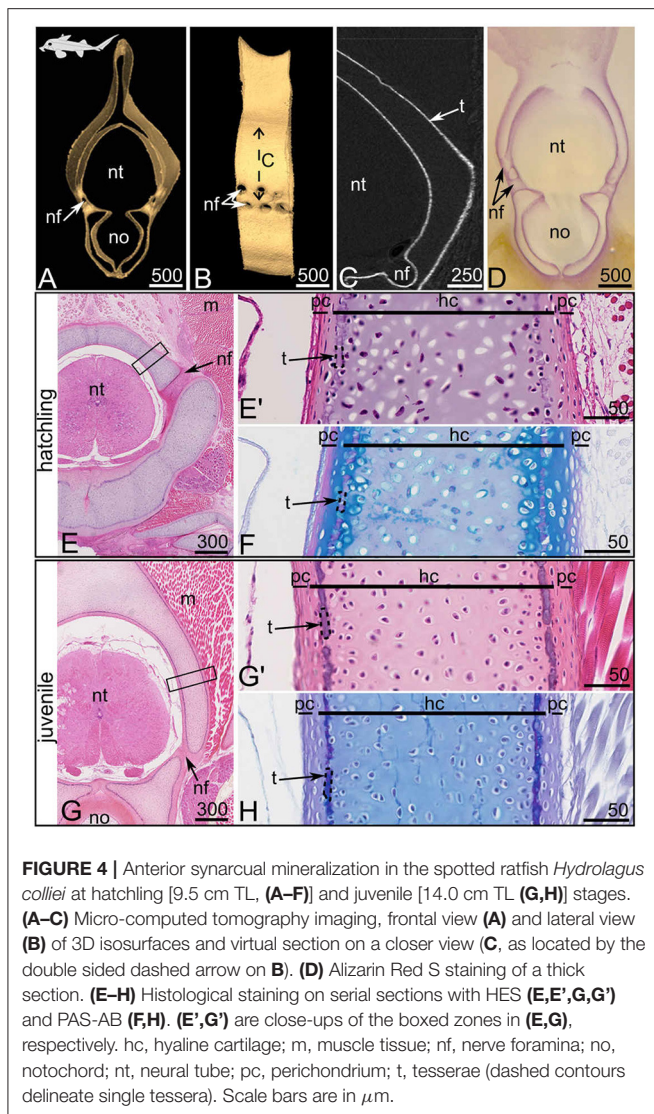mineralized perichondrium (toward the trunk muscles) with the

FIGURE 4 | Anterior synarcual mineralization in the spotted ratfish *Hydrologus colliei* at hatchling [9.5 cm TL, **(A–F)**] and juvenile [14.0 cm TL **(G,H)**] stages. **(A–C)** Micro-computed tomography imaging, frontal view **(A)** and lateral view **(B)** of 3D isosurfaces and virtual section on a closer view **(C**, as located by the double sided dashed arrow on **B)**. **(D)** Alizarin Red S staining of a thick section. **(E–H)** Histological staining on serial sections with HES **(E,E',G,G')** and PAS-AB **(F,H)**. **(E',G')** are close-ups of the boxed zones in **(E,G)**, respectively. hc, hyaline cartilage; m, muscle tissue; nf, nerve foramina; no, notochord; nt, neural tube; pc, perichondrium; t, tesserae (dashed contours delineate single tessera). Scale bars are in μm.

proximal mineralized perichondrium (facing the neural tube) (compare **Figures 2C1,C3,D1,D3**).

As a result, three mineralized histotypes can be described in the neural arch of *S. canicula*. The first one is superficial lamellar mineralization that arises from the perichondrium located in the proximal side of the neural arch. The mineralized matrix displays a lamellar organization, cell density appears very low, and the few cells found in the mineralized matrix are elongated (**Figures 2C1,D1**). The second type is globular mineralization, which occurs in the matrix surrounding chondrocytes in the dorsal part of the neural arch and the contact zone with perichondrial mineralized tissues. HES staining in the mineralized matrix shows concentric rings around the chondrocyte lacunae that we interpret as the marks of previously described Liesegang lines (**Figure 2C2**), typical of globular mineralization in hyaline cartilage (Ørvig, 1951; Peignoux-Deville et al., 1982; Seidel et al., 2016). The pericellular space is positive for Alcian blue (ps in **Figure 2D2**). The third type is a

fibrous mineralized tissue in the perichondrium that is located in the distal side of the neural arch. The cells also appear elongated as expected with fibrocytes and their matrix is characterized by loosely arranged fibers that stain with Saffron (arrows in **Figure 2C3**). The thin pericellular space is positive for Alcian blue (**Figure 2D3**).

3.1.2. Neural Arch Mineralization in *Raja clavata*

The posterior vertebrae of *R. clavata* are composed of a centrum associated with one neural arch located dorsally, at the junction between two neural spine-interdorsal complexes (**Figures 3A,B**). The neural arches and interneural elements are not covered by tesserae, as opposed to the neural spines (**Figure 3B**). The virtual section shows that the whole depth of the posterior neural arches is mineralized (**Figure 3C**). In both hatchling and juvenile specimens, this architecture is similar in the posterior vertebral column (not shown). HES histological staining highlights the presence of subspherical cells in the center of these neural arches (**Figures 3I',J,N',O,N2,O2**). Their extracellular matrix displays Liesegang lines with HES and an Alcian blue positive pericellular space with PAS-AB, making this zone similar to the globular mineralization observed in *S. canicula* (**Figures 3N2,O2**). This internal mineralized cartilaginous rod does not seem to differ in size between the hatchling and juvenile specimens, suggesting little growth of this internal zone between the corresponding ontogenetic stages (**Figure 3**, compare the g zone in I' with N').

Surrounding this mineralized cartilage core is a tissue with fibrocyte-shaped cells, engulfed in a fibrous matrix devoid of Alcian blue staining except for a thin pericellular matrix (**Figures 3I',J,N',O,N1,N3,O1,O3**). This mineralized fibrous tissue lines both the proximal and distal sides of the neural arch and is thicker in the juvenile than in the hatchling specimen (compare **Figures 3I',N'**). We assume this tissue to have a perichondrial nature, and it appears similar to the fibrous mineralization in the distal perichondrium of the *S. canicula* neural arches. Similar to the observations in *S. canicula*, perichondrial mineralization appears denser than globular cartilage mineralization (**Figure 3C**). In contrast to *S. canicula*, no lamellar organization of the extracellular matrix was observed in either the proximal or distal perichondrium of *R. clavata* (**Figures 3N1,N3,O1,O3**). In *S. canicula*, the architecture of neural arch mineralization is the same along the anterior-posterior axis of the vertebral column (no difference is observed between the anterior and posterior vertebrae) although the timing of centrum mineralization differs between these regions (Enault et al., 2016). In *R. clavata*, the mineralization architecture in the neural arches differs between anterior and posterior vertebrae (**Figures 3B,F**). In anterior vertebrae, we identified only interneural elements, located dorsal to the junctions between two centra and that were partly covered with tesserae (**Figures 3F,H**), while more massive mineralized units cover the anterior and posterior faces of the interneural elements (**Figures 3F,K**). A longitudinal frontal section in an interneural element shows that these massive units have a U-shape delineating the anterior and posterior faces of each interneural element (**Figure 3K**). As such, we considered them to be "corner tesserae" as previously proposed in the jaw of
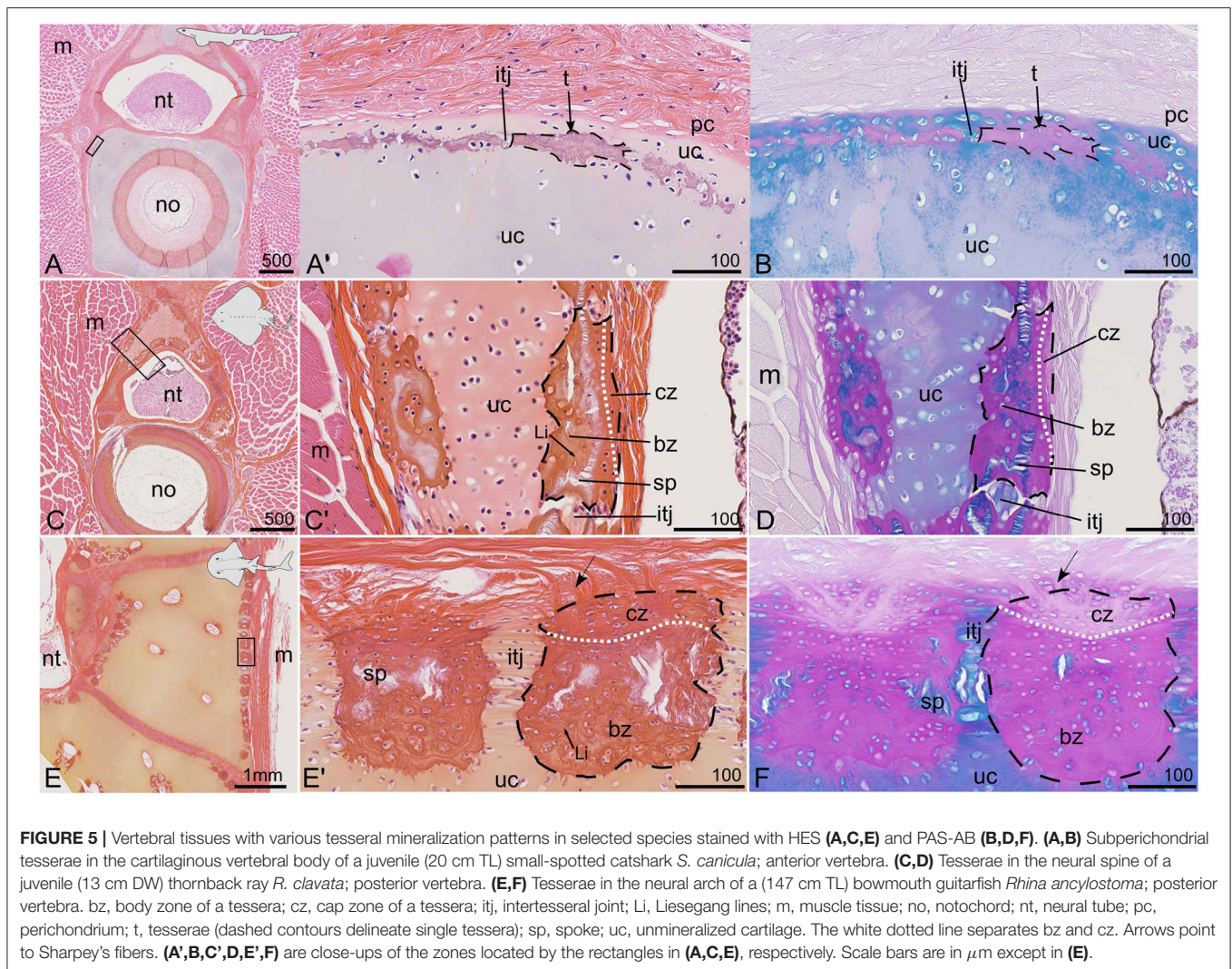
FIGURE 5 | Vertebral tissues with various tesseral mineralization patterns in selected species stained with HES **(A,C,E)** and PAS-AB **(B,D,F)**. **(A,B)** Subperichondral tesserae in the cartilaginous vertebral body of a juvenile (20 cm TL) small-spotted catshark *S. canicula*; anterior vertebra. **(C,D)** Tesserae in the neural spine of a juvenile (13 cm DW) thornback ray *R. clavata*; posterior vertebra. **(E,F)** Tesserae in the neural arch of a (147 cm TL) bowmouth guitarfish *Rhina ancylostoma*; posterior vertebra. bz, body zone of a tessera; cz, cap zone of a tessera; itj, intertesseral joint; Li, Liesegang lines; m, muscle tissue; no, notochord; nt, neural tube; pc, perichondrium; t, tesserae (dashed contours delineate single tessera); sp, spoke; uc, unmineralized cartilage. The white dotted line separates bz and cz. Arrows point to Sharpey's fibers. **(A',B,C',D,E',F)** are close-ups of the zones located by the rectangles in **(A,C,E)**, respectively. Scale bars are in μm except in **(E)**.

the Haller's round ray *Urobatis halleri* (Dean et al., 2009), although their size relative to the closest tesserae is higher than that of previously observed "corner tesserae" (**Figure 3F**). Histological staining showed the occurrence of mineralized globular cartilage in the center of these elements and layers of fibrous perichondrial mineralization on their proximal and distal surface (**Figures 3L,M**).

As a consequence, the interneural elements and neural arches of *S. canicula* and *R. clavata* in the caudal zone of the vertebral column display continuous mineralization, while the anterior vertebrae of *R. clavata* (immediately posterior to the synarcual) display a combination of tesserae and massive "corner tesserae". All these mineralized structures are characterized by a mineralized perichondrial tissue that covers a partly (*S. canicula*) or more extensively (*R. clavata*) mineralized cartilaginous rod. Perichondrial mineralization occurs as lamellar mineralization only in the proximal zone of the neural arches of *S. canicula* and as fibrous mineralization in all other occurrences.

3.1.3. Synarcual Mineralization in *Hydrolagus colliei*

The synarcual of *H. colliei* is a post-cranial element pierced by dorsal and ventral nerve foramina (**Figures 4A,B**) that develops from the fusion of successive embryonic vertebrae and that does not display discrete neural arch or interneural elements (Johanson et al., 2015). The equivalent zone of elasmobranch neural arches in the synarcual is considered to be the zone dorsal to a ventral foramen (Goodrich, 1930; Eames et al., 2007; Criswell et al., 2017). We hypothesized a similar situation for chimaeras, and focused on the portion of the synarcual located dorsally to a ventral foramen, although our observations were similar in all other parts of the synarcual (including in the vertebral body, see **Figures 4A,D,E,G**). Previous studies showed poorly developed cartilaginous tissue in the posterior vertebrae of juvenile *H. colliei*, where histology displayed no sign of modified cartilaginous matrix that could be linked to cartilage mineralization (Debiais-Thibaud, 2019). However, more recent publications pointed out the thin layer of mineralized matrix in the synarcual of the elephant shark *Callorhinchus milii* (Pears

et al., 2020) and recognized thin tesserae in the adult *C. milii* and rabbit fishes *Chimaera monstrosa* (Pears et al., 2020; Seidel et al., 2020). In our *H. colliei* sample, we detect a similar thin layer of mineralized tissue in the synarcual of a hatchling and a juvenile specimen (**Figures 4A,G**). This pattern is found as a peripheral delineation of the ventral part (corresponding to the vertebral body) and the dorsal part (corresponding to the neural arches) of the synarcual, but also in the inner contact with the notochord (**Figures 4A,D,G**). Most tesserae are not more than 10 μm wide in their chondral-perichondral axis (**Figures 4E',F,G',H**). The line of modified cartilaginous matrix can be observed at the hatching stage and is more obvious in the juvenile specimen (**Figures 4E–H**). The matrix stains deep purple with HES (**Figures 4E',G'**) and does not stain with Alcian blue (**Figures 4F,H**), suggesting a difference in the glycosaminoglycan content at this mineralization location. This site of mineralization is located in the subperichondrial zone of the cartilaginous unit. The cells located on the perichondrial side of this line are enclosed in lacunae in a matrix of cartilaginous nature [as supported by positive Alcian blue staining (**Figures 4F,H**)], although the cells are flattened (**Figures 4E',G'**). Moreover, no cells can be observed fully embedded in the mineralized cartilaginous matrix, either at the hatching or juvenile stage and the mineralized layer appears discontinuous (**Figures 4G',H**), supporting the presence of aligned tesserae as described in other holocephalan species (Pears et al., 2020).

3.1.4. Diverse Combinations of Histotypes in Chondrichthyan Tesserae

To better compare our observations with literature data on tesserae, these mineralized structures were also illustrated in selected species (**Figure 5**). As previously noted, focal cartilage mineralization is detected with microCT outside the neural arches and surrounding the vertebral body of *S. canicula* (**Figures 1A,B**). Such sites also appear on histology sections, they are stained dark pink with HES and purple with PAS-AB and occur in a subperichondrial location within the cartilaginous matrix (**Figures 5A,B**). Although poorly developed, these sites can be interpreted as thin tesserae engulfing chondrocytes and display intertesseral joint regions (**Figures 5A',B**), as previously described (Seidel et al., 2016). The tesserae are separated from the perichondrium by a subperichondrial and unmineralized cartilaginous layer (**Figures 5A',B**). They are comparable to the discontinuous pattern of mineralization described in *H. colliei* (**Figures 4G',H**) but are thicker (up to 50 μm) and engulf chondrocytes in the mineralized matrix (**Figure 5A'**) in *S. canicula*.

The neural spines of *R. clavata*, as well as the neural arches of the bowmouth guitarfish *Rhina ancylostoma* are covered by tesserae (**Figures 3B, 5C–F**). The tesserae are separated by unmineralized intertesseral joints (itj in **Figures 5C',D,E',F**) and display internal spokes (sp in **Figures 5C',D,E',F**) as defined by Seidel et al. (2016). Two zones can further be distinguished in the tesserae that correspond to the previously defined body and cap zones of a tessera (Kemp and Westrin, 1979; Seidel et al., 2016, 2017). In both species, the cap zone is characterized by flat cells, a higher content in collagen fibers, and a matrix poorly stained by

Alcian blue except in the pericellular layer (**Figures 5D,F**). The cells in the body zone are subspherical and surrounded by an extracellular matrix displaying Liesegang lines with HES staining (**Figures 5C',E'**). In both batoids (*R. clavata* and *R. ancylostoma*), the maximum width of a tessera (tangential axis) is about 200 μm and does not seem to depend on the specimen body size as *R. clavata* is a young juvenile of 13 cm DW and 21 cm TL, while *R. ancylostoma* is 147 cm long. However, the depth of the tesserae (along the chondral-perichondral axis) is less than 100 μm in *R. clavata*, while it is more than 200 μm in *R. ancylostoma* (compare **Figures 5D,F**). There are no obvious Sharpey's fibers radiating from the tesserae of *R. clavata*, whereas they are well-defined in the tesserae of *R. ancylostoma* (**Figures 5C',D,E'F**). Sharpey's fibers are thick collagenous fibers previously described in tesserae (Kemp and Westrin, 1979; Seidel et al., 2017).

3.2. Neural Arch Mineralization and Elasmobranch Diversity

In the following, we describe the variation of neural arch mineralized histotypes and architectures in several species covering a broad part of the elasmobranch taxonomic diversity.

3.2.1. Batoids

Most of the neural arch of the smooth butterfly ray *Gymnura micrura* and *Torpedo* sp. is covered by tesserae that are 250 μm wide in their tangential axis (**Figures 6A,B,E,F**). Two larger mineralized elements are found on the anteriormost and posteriormost surfaces of each neural arch, similar to the corner tesserae described in *R. clavata*. These elements are more than 500 μm in their longer dimension (**Figures 6A,E**). The virtual sections made through the center of the neural arches show regular-sized tesserae on the neural arch surface (**Figures 6B,F**). The histological sections made through the corner tesserae (**Figures 6C,G**) show a central zone of globular mineralized cartilage covered by fibrous mineralization (**Figures 6C,D,G',H**).

The neural arches of the shovelnose guitarfish *Pseudobatos productus* are covered by classically organized tesserae with no massive corner tesserae (**Figure 6I**). The tesserae of the neural arch reach 400 μm long (in their tangential axis) and 100 μm wide (along the chondral-perichondral axis, **Figure 6J**) and display intertesseral joints (**Figures 6K',L**). The cap zone of a tessera contains elongated cells in a fibrous (Saffron-positive) matrix with little acidic glycosaminoglycan content (**Figures 6K',L**), while cells in the body zone are similar in shape to chondrocytes in the unmineralized matrix (**Figures 6K',L**). The neural arch of *R. ancylostoma* also is covered by standard tesserae only (**Figures 6E,F**) without enlarged elements (data not shown).

3.2.2. Selachians, Squalomorphs, Order: Squaliformes

In both the velvet belly *Etmopterus spinax* and the longnose velvet dogfish *Centroscymnus crepidater*, the neural arches display thin zones of mineralization dorsal to the centra (**Figures 7A,B,E,F**). Virtual sections passing through the neural arches show a thin, discontinuous layer of mineralization (**Figures 7B,F**). The histological staining results show that the
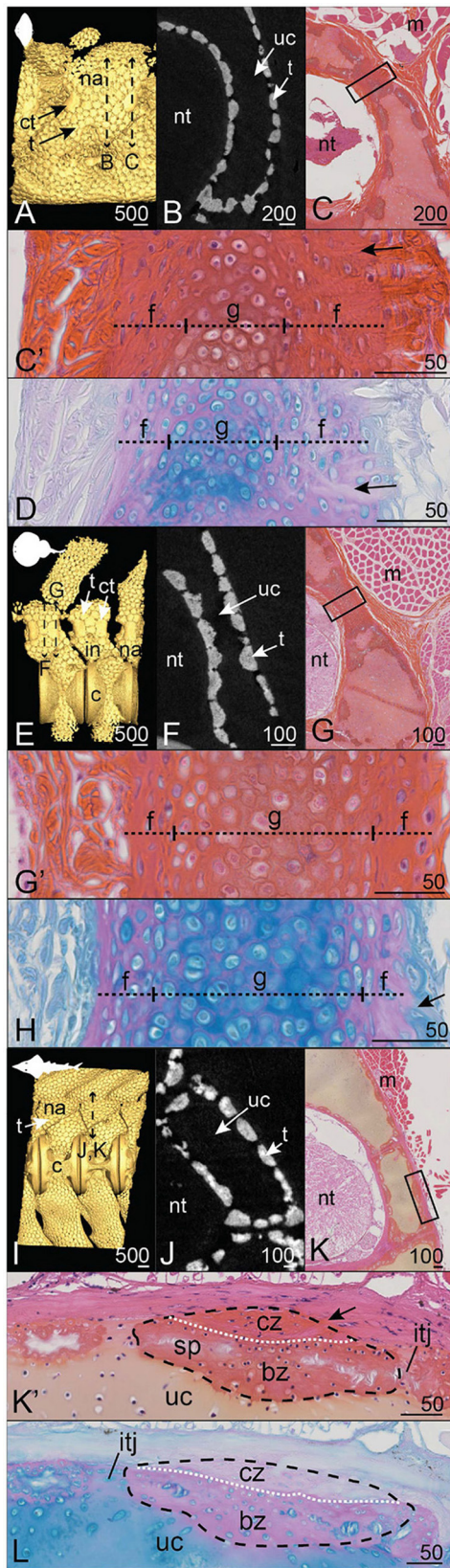
FIGURE 6 | Mineralization patterns in the neural arches of posterior vertebrae in batoids. (A–D) Smooth butterfly ray *Gymnura micrura* (40.5 cm DW). (E–H) *Torpedo* sp. (16 cm DW). (I–L) Shovelnose guitarfish *Pseudobatos productus* (60 cm TL). (A,E,I) 3D isosurfaces. (B,F,J) Virtual cross sections following the plane indicated by the double sided dashed arrow in (A,E,I). (C,G,K) HES staining on transverse sections following the plane indicated by the double sided dashed arrow in (A,E,I). (C',G',K') Close-ups of the boxes in (C,G,K). (D,H,L) PAS-AB staining of similar zones as in (C',G',K'), respectively. Legends as in **Figures 1–5**.

thin mineralization layer is both proximal (facing the neural tube) and subperichondral (**Figures 7C,D,G,H**). Although the majority of the neural arch is composed of unmineralized cartilage matrix containing round chondrocytes (**Figures 7D,H**), the HES staining shows thin purple-stained blocks within the cartilaginous matrix that do not embed any cells (**Figures 7C',G'**), similar to the thin tesserae described in *H. colliei*. The tesserae are 10 μm wide (in their chondral-perichondral axis, **Figures 7C',G'**) and are separated from the neural tube by a layer of cartilaginous matrix in *C. crepidater* (**Figure 7G'**), while it occurs in contact with the very thin perichondrium in *E. spinax* (**Figure 7C'**).

3.2.3. Selachians, Squalomorphs, Order: Squatiniformes

In the Pacific angelshark *Squatina californica*, the dorsal neural arches and interneural elements appear as continuously mineralized structures that are contiguous with the tesserae covering the neural spine and the basidorsal and basiventral elements (**Figure 8I**). The virtual section of the *S. californica* vertebra shows an internal variation in the mineral density of this structure, with denser peripheral mineralization than in the core (**Figure 8J**). On the histological sections, the cartilaginous tissue core contains round chondrocytes in a modified matrix (**Figures 8K',L**), similar to our previous description of globular mineralization. This central cartilaginous zone is covered proximally and distally by a fibrous mineralized tissue that contains flattened cells, similar to what we already described for fibrous mineralization of the perichondrium (**Figures 8K',L**).

3.2.4. Selachians, Galeomorphs, Order: Carchariniformes

In all three Carchariniformes considered in the following, neural arch and interneural mineralization builds up continuous structures (**Figures 8A,E,I**). Neural arch mineralization is ventrally contiguous with tesserae from the vertebral body in the tope shark *Galeorhinus galeus* and the scalloped hammerhead *Sphyrna lewini* (**Figures 8A,B,E,F**).

The continuously mineralized elements of *G. galeus* and *S. lewini* include neural arches and interneural elements (**Figures 8A,E**). In both species, neural arch mineralization encloses an unmineralized core and appears denser on the proximal and distal faces than on the dorsal zone (**Figures 8B,F**). The dorsal zone and the contact zone with the mineralized perichondrium are composed of globular mineralization (g in **Figures 8C',D,G',H**). The perichondrial layer of the mineralized tissue is similar to the fibrous mineralization sites described in the
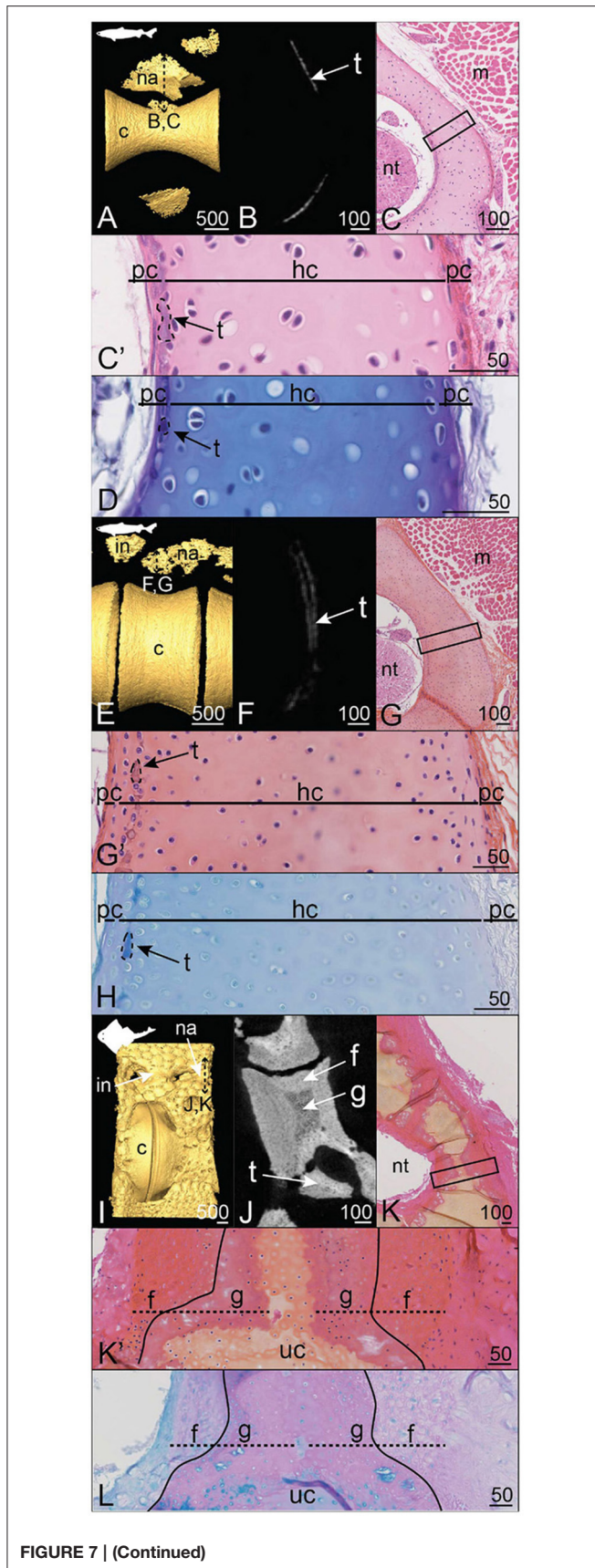
FIGURE 7 | Mineralization patterns in the neural arches of posterior vertebrae in Squaliformes. **(A–D)** Velvet belly *Etmopterus spinax* (23 cm TL). **(E–H)** Longnose velvet dogfish *Centroscymnus crepidater* (31 cm TL). **(I–L)** Pacific angelshark *Squatina californica* (75 cm TL). **(A,E,I)** 3D isosurfaces. **(B,F,J)** Virtual cross sections following the plane indicated in **(A,E,I)**, respectively. **(C,G,K)** HES staining on transverse sections following the plane indicated in **(A,E,I)**. **(C',G',K')** Close-ups of the boxes in **(C,G,K)**. **(D,H,L)** PAS-AB staining of similar zones as in **(C',G',K')**, respectively. Legends as in **Figures 1–5**.

distal side of the *S. canicula* neural arch, with enclosed fibrocyte-shaped cells and no observable lamellae (**Figures 8C',D,G',H**).

In the blue shark *Prionace glauca*, neural arch and interneural mineralization sites alternate dorsal to the large centrum and no tesserae can be observed on the whole vertebral unit (**Figure 8I**). Mineralization is very restricted to the dorsoventral axis of the neural arch. The neural arch mineralization is superficial to only one location of the unmineralized cartilaginous neural arch (**Figure 8K**). The mineralized tissue includes globular mineralization in its innermost zone, together with outer perichondral layers on both proximal and distal sides of the neural arch (**Figures 8K',L**). These perichondral layers are not homogeneous because the cells undergo a morphological transition from flat—in the contact zone with globular mineralization—to subspherical—in the external zone (**Figures 8K',L**). Besides, the extracellular matrix of the external zone shows HES and Alcian blue staining similar to unmineralized cartilage, suggesting the presence of hyaline cartilaginous matrix in this perichondral zone (**Figures 8K',L**). However, this external layer also displays numerous bundles of collagen fibers similar to Sharpey's fibers (**Figure 8K'**). The progressive centrifugal transition from a fibrous to a cartilaginous nature of the outer layers corresponds to a progressive decrease of mineralization, as shown in the virtual section (**Figure 8J**).

3.2.5. Selachians, Galeomorphs, Orders: Heterodontiformes, Orectolobiformes, and Lamniformes

In the horn shark *Heterodontus francisci* and the brownbanded bambooshark *Chiloscyllium punctatum*, alternate neural arches and interneural elements display a fully mineralized surface (**Figures 9A,E**). Tesseral mineralization is also located ventral to the neural and interneural elements of *H. francisci* (**Figure 9A**). In both species, the neural arch displays an unmineralized central core (**Figures 9B,F**) made of cartilage (**Figures 9C',G'**). However, globular mineralization is detected in the cartilaginous core in contact with the mineralized perichondral layers (**Figures 9C',G'**). In *H. francisci*, the perichondral mineralized layers are highly fibrous, in particular in the distal layer where numerous Sharpey's fibers are observed and incorporate numerous flattened cells (arrows, **Figures 9C',D**). On the contrary, the proximal perichondrium of the *C. punctatum* neural arch contains very few cells and the matrix is arranged in lamellae (**Figures 9G',H**). Overall, the organization and composition of the *C. punctatum* neural arch are very similar to what is observed in the *S. canicula* neural arch (compare with **Figures 1C, 2A',B,C',D**).
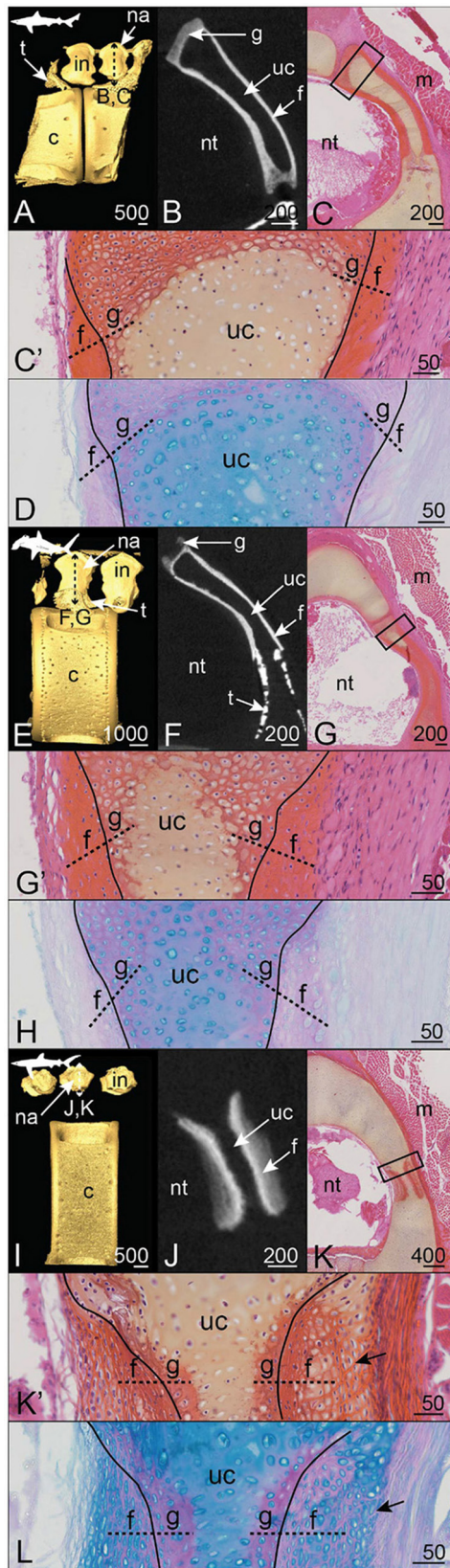
FIGURE 8 | Mineralization patterns of the neural arches in Carcharhiniformes. (A–D) Anterior vertebra of a tope shark *Galeorhinus galeus* (50 cm TL). (E–H) Posterior vertebra of a scalloped hammerhead *Sphyrna lewini* (60 cm TL). (I–L) Posterior vertebra of a blue shark *Prionace glauca* (80 cm TL). (A,E,I) 3D isosurfaces. (B,F,J) virtual cross sections following the plane indicated in (A,E,I). (C,G,K) HES staining on transverse sections following the plane indicated in (A,E,I) (C',G',K') Close-ups of the boxes in (C,G,K). (D,H,L) PAS-AB staining of similar zones as in (C',G',K'), respectively. Legends as in **Figures 1–5**.

FIGURE 8 | (Continued)

The neural arch of the bull shark *Carcharias taurus* displays superficial mineralization in the form of standard size tesserae, while the core of the neural arch remains unmineralized (**Figures 9I,J**) and cartilaginous (**Figure 9K**). The tesserae are about 300 μm long (tangential axis) and 150 μm wide (along the chondral-perichondrial axis, **Figures 9K',L**). The cap and body zones cannot be properly distinguished from our sample, probably because of a tilted section plan (**Figures 9K',L**). However, we observe Sharpey's fibers anchoring the tesserae to the distal fibrous layer of the neural arch (arrows, **Figures 9K',L**) and unmineralized intertesseral joints (**Figures 9K',L**).

4. DISCUSSION

In the following, we discuss our results at two scales of organization, as previously defined by Dean and Summers (2006). The description of the cells and extracellular matrices involved in the mineralization (microscale description) allows defining three histotypes: globular mineralization (as reported by Ørvig, 1951), fibrous mineralization, and lamellar mineralization (as reported by Peignoux-Deville et al., 1982). On the other hand, the description of the whole skeletal elements (mesoscale description) provides insights into three mineralization architectures: discontinuous with tessellated cartilage, continuous over the whole neural arch, and semi-discontinuous in which tesserae are found associated with larger elements that we herein named corner tesserae.

4.1. Microscale Characterization of the Diversity of the Chondrichthyan Mineralized Tissues

In this work, we described the distribution of three histotypes in the neural arches of a wide taxonomic range of cartilaginous fishes. These results highlight the combined contribution of cartilaginous and perichondrial tissues in building the mineralized skeletal units of most chondrichthyans.

First, we identified globular mineralization that initiates in the hyaline cartilaginous matrix of the neural arches of all sampled species, in all architectures. It occurs in poorly developed tesserae of a holocephalan and the two Squaliformes examined in this study, in the body zone of tesserae of several elasmobranch species, in the most internal layer of the corner tesserae, and in the continuously mineralized neural arches of the other species. The classical description of tessellated cartilage includes such globular mineralization in the body zone (Kemp and Westrin, 1979; Seidel et al., 2016, 2017; Maisey et al., 2020), where the
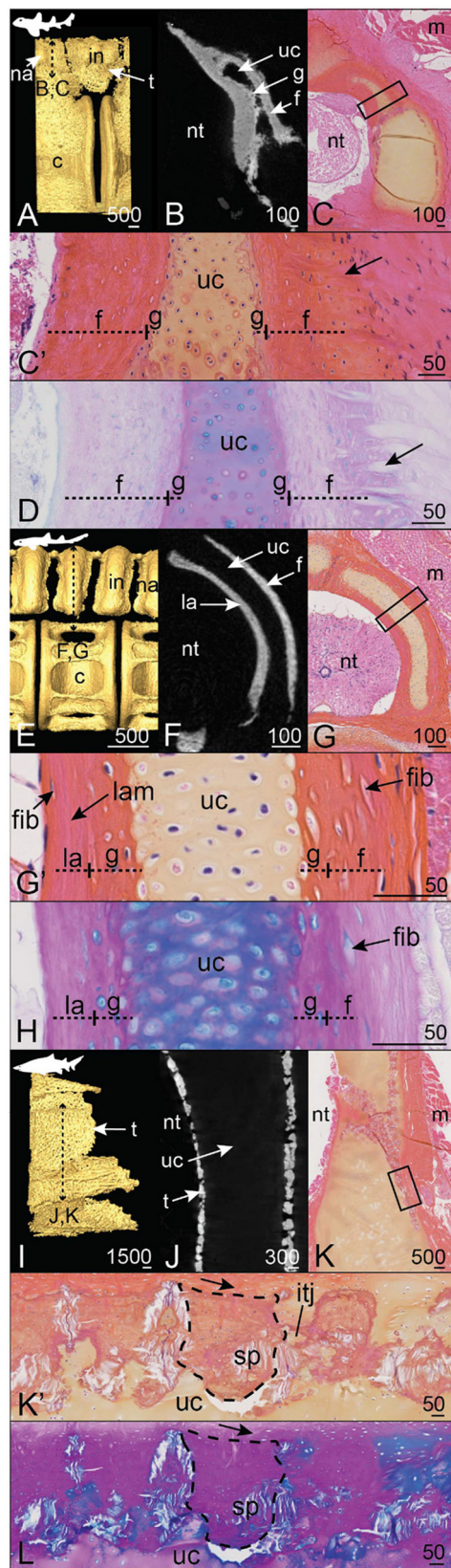
FIGURE 9 | Mineralization patterns of the neural arches in galeomorphs (excluding Carcharhiniformes). (A–D) posterior vertebra of a horn shark *Heterodontus francisci* (55 cm TL). (E–H) Anterior vertebra of a brownbanded bambooshark *Chiloscyllium punctatum* (19.3 cm TL). (I–L) Anterior vertebra of a bull shark *Carcharias taurus* (270 cm TL). (A,E,I) 3D isosurfaces. (B,F,J) Virtual cross sections following the plane indicated in (A,E,I). (C,G,K) HES staining on transverse sections following the plane indicated in (A,E,I). (C',G',K') Close-ups of the boxes in (C,G,K). (D,H,L) PAS-AB staining of similar zones as in (C',G',K'), respectively. Legends as in **Figures 1–5**.

surrounding matrix is hyaline and cells display a chondrocyte morphology with some shape variations (Chaumel et al., 2020). In both standard and corner tesserae, our observations are consistent with globular mineralization, from the observation of heterogeneous staining marking the presence of Liesegang lines. Although the exact nature of these Liesegang lines is not clear, they were hypothesized to be produced by the rhythmic activity of chondrocytes in their matrix (Kemp and Westrin, 1979). Because chondrocytes are not embedded in the mineralized matrix of the poorly developed tesserae of *E. spinax*, *C. crepidater*, and *H. colliei*, we could not detect Liesegang lines. However, Liesegang lines have been described in the thin tesserae of other holocephalan species (Pears et al., 2020; Seidel et al., 2020), defining these tesserae as sites of globular mineralization. Previous studies also showed that fully developed tesserae first appear only as subperichondrial focal mineralization sites (Enault et al., 2015; Seidel et al., 2016). This suggests that tesserae remain in an "under-developed" stage in holocephalan species as they do not engulf chondrocytes and are devoid of cap zone mineralization (Pears et al., 2020; Seidel et al., 2020), although chondrocytes in the mineralized matrix were described at an early stage of tesseral growth in *C. milii* (Pears et al., 2020). Our findings extend the occurrence of this thin globular mineralization outside of holocephalans, in selachian species with secondarily poorly mineralized skeletons (*E. spinax* and *C. crepidater*) but also in sites of poor development of these tesserae (in the *S. canicula* vertebral body).

Although they did not study and precisely describe neural arches, Ridewood and MacBride (1921) first illustrated several transverse sections of vertebrae that showed the diversity of mineralized tissues in elasmobranchs. More recent studies have interpreted some aspects of the mineralized neural arch tissues as "bone-like" in few elasmobranch species (Eames et al., 2007; Enault et al., 2015; Atake et al., 2019). Here we show that such tissues may be of at least two different types that we both hypothesize to be of perichondrial origin. Of these two types, fibrous mineralization is found in all occurrences of a continuously mineralized neural arch, is defined by the presence of fibrocyte-shaped cells enclosed in a fibrous matrix often crossed by Sharpey's fibers, and stands in continuity with the peripheral unmineralized connective tissue that links the neural arches to the surrounding muscles. Our histological results support a perichondrial nature of the tissue and therefore a growth by external apposition, as previously suggested (Atake et al., 2019). Also, we show that the inner cartilaginous core keeps a stable thickness in embryonic and

juvenile stages of development, supporting the fact that growth of the outer layers of the neural arches is generated through the activity of perichondrial cells (**Figures 2**, **3**). In our histological assays, there is no staining difference between the fibrous continuous mineralization in neural arches and the cap zone of fully developed tesserae. The cap zone has classically been described as a tissue with a derived type of mineralization (prismatic mineralization in Ørvig, 1951). Because prismatic mineralization can only be identified through polarized light microscopy, our sample preparation does not allow identifying the prismatic nature of the observed mineralization. However, the perichondrial characteristics of the cap zone have also been discussed recurrently in both the continuous neural arch tissues and the cap zone of tesserae because of the presence of type I collagen fibers and the observation of fibrocyte-shaped cells (Kemp and Westrin, 1979; Dean and Summers, 2006; Seidel et al., 2017). Further comparison to bone tissue was also often raised about the cap zone because of its dense mineralization and because of its topological location, similar to the perichondrial bone described in early vertebrates (Ørvig, 1951; Donoghue and Sansom, 2002). In our microCT images, we also detected internal variation of mineral density, suggesting lower density in globular mineralization as compared to fibrous mineralization. A more detailed tissue characterization, including recognition of cellular and lacunar shape or density, would have involved microCT scans of a much higher resolution than those analyzed here.

The third mineralized tissue identified in our samples is another type of perichondrial tissue that we named lamellar mineralization and that is only observed on the proximal side of the neural arches of *S. canicula* and *C. punctatum*. This lamellar tissue in *C. punctatum* is thin and our sampled individual was a young juvenile (19.3 cm TL) so it remains difficult to be properly compared to our observation in *S. canicula*. In *S. canicula*, the extracellular matrix content of this tissue appears more linearly organized than in fibrous mineralization (hence the lamellar denomination). The cell density is extremely low as compared to both cartilaginous and fibrous tissues and the rare cells observed in the matrix are similar to fibrocytes encased in the lamellar matrix, which is particularly visible in the elder *S. canicula* sample (**Figures 1C',D,C1,D1**). The growth of this tissue has to be appositional from cells located on the proximal surface of the neural arch, facing the neural tube, where no thick unmineralized perichondrium was apparent in our samples but only a monolayer of fibrocytes (see **Figure 9G'**). This observation highlights the potential for very different growth processes between the fibrous and lamellar mineralized tissues, as cells do not seem to behave similarly, being either engulfed and kept alive (distal side) or dead or excluded from the mineralized matrix (proximal side).

4.2. Mesoscale Mineralization Patterns: Continuous vs. Discontinuous Architectures

At mesoscale, we chose to classify our observations into several types. We defined the mineralization architecture as discontinuous when the neural surface is covered by tesserae of homogeneous size, either fully developed with a body and

cap zones (Dean et al., 2009; Seidel et al., 2020) as in *C. taurus* and in Rhinopristiformes, or reduced in size and acellular (Maisey et al., 2020; Pears et al., 2020) as in Squaliformes and in *H. colliei* (**Table 2** and **Figure 10**, yellow silhouettes). We further observed discontinuous architecture in the neural arches of the posterior vertebrae of another batoid (in the white-blotched river stingray *Potamotrygon leopoldi*, data not shown). On the opposite extreme, we termed continuous architecture the neural arch surface that is mineralized as a whole (**Figure 10**, green silhouettes). Continuous mineralization involves globular, fibrous, and eventually lamellar mineralizations and is reported in Squatiniformes, Rajiformes, and all galeomorphs except in Lamniformes (**Table 2** and **Figure 10**, green silhouettes).

The third mesoscale architectural pattern is characterized by the co-occurrence of homogeneous tesserae covering most of the neural arch surface in addition to two larger elements located on the anteriormost and posteriormost sides of the neural arch, which we named corner tesserae after Dean et al. (2009). From histology, these large elements are comparable both to tesserae and to continuously mineralized neural arches because they involve an internal (chondral) globular mineralization and an external (perichondral) fibrous mineralization. However, they differ from standard tesserae because of their size and also because they cover the surface of the proximo-distal face of the element, in addition to having two parallel faces, one on the proximal surface and the other one on the distal surface of the neural arch, making them U-shaped in their anterior-posterior axis (**Figure 3K**). As a result, they could be interpreted either as highly modified and enlarged tesserae, or as continuous mineralization that is restricted to only part of the neural arch surface. We termed this situation a semi-discontinuous architecture, considering it an intermediate state between discontinuous and continuous architectures (**Figure 10**, red silhouettes).

We described the semi-discontinuous architecture only in batoids, in the posterior vertebrae of *G. micrura* (Myliobatiformes) and *Torpedo* sp. (Torpediniformes) (**Table 2** and **Figure 10**, red silhouettes). Besides, we report its occurrence in the anterior vertebrae of *R. clavata* (Rajiformes), whereas the posterior vertebrae displayed continuous mineralization. Within Rajiformes, a semi-discontinuous architecture was reported in the Eaton's skate anterior vertebrae *Bathyraja eatonii* (Rajiformes) (Atake et al., 2019), while continuously mineralized neural arches were observed in the little skate posterior vertebrae *Leucoraja erinacea* (Criswell et al., 2017). The co-occurrence of continuous and semi-discontinuous architectures in *R. clavata* calls for more complete descriptions of the mineralized structures in vertebral columns in a wider range of Rajiformes, and other batoids, to allow making any inference on the ancestral state of mineralization architecture in this group.

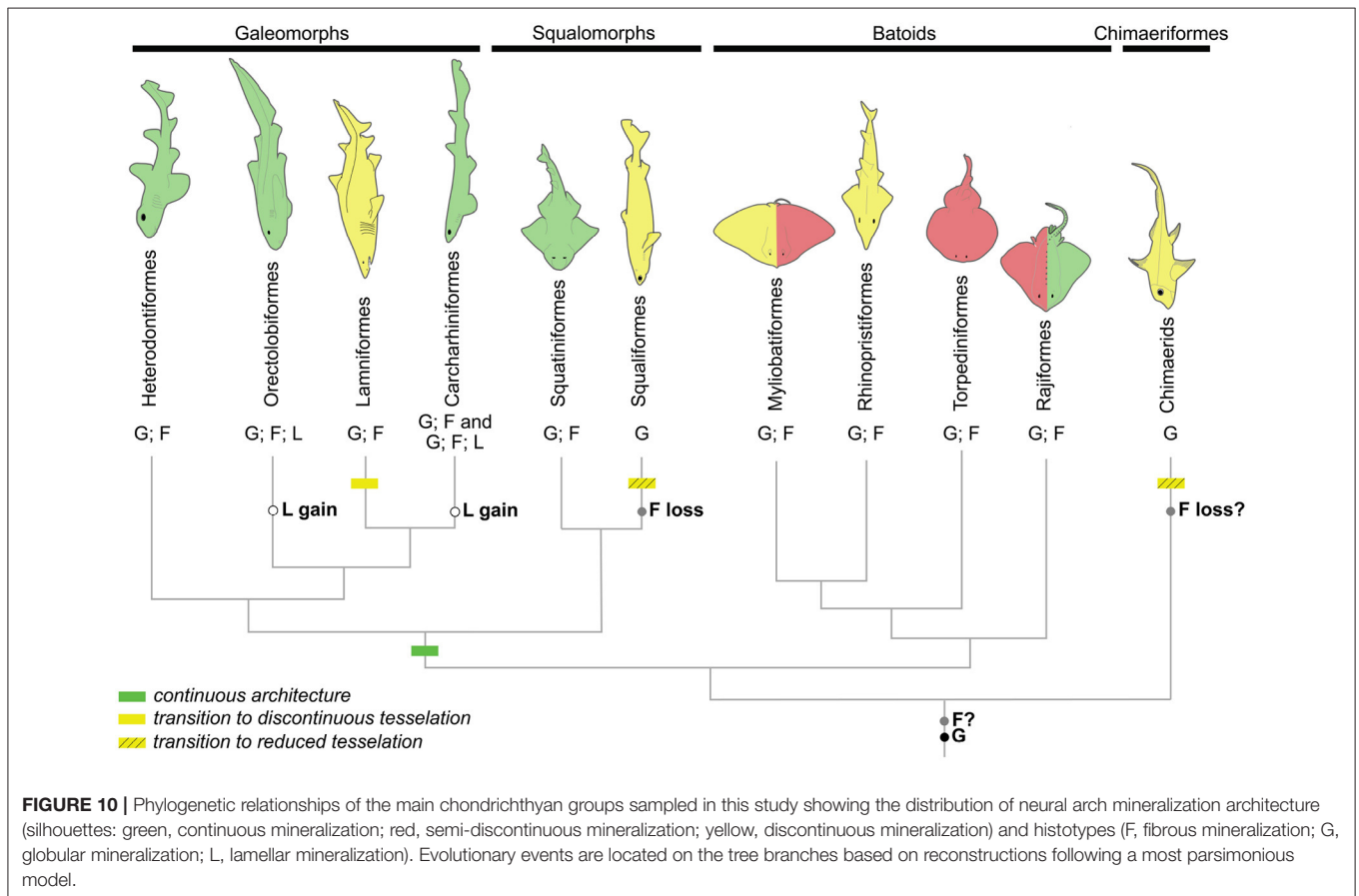## 4.3. Prospects on the Evolution of Mineralized Histotypes in Vertebrates
4.3.1. The Putative Nature of Fibrous Mineralization
Our work provides a histological examination in an unprecedented taxonomic range of elasmobranch fishes. We uncover the occurrence of fibrous mineralization in

TABLE 2 | Description and categorization of the mineralized tissues in the neural arches of the chondrichthyan species examined in this study.

Species	Order	Mineralization histotypes (microscale)			Mineralization architecture (mesoscale)
		Globular (c)	Fibrous (pc)	Lamellar (pc)	
S. canicula	Carcharhiniformes	+	+, dist	+, prox	
C. punctatum	Orectolobiformes	+	+, dist	+, prox	
P. glauca	Carcharhiniformes	+	+	−	
G. galeus	Carcharhiniformes	+	+	−	Continuous
S. lewini	Carcharhiniformes	+	+	−	
H. francisci	Heterodontiformes	+	+	−	
S. californica	Squatiniformes	+	+	−	
R. clavata	Rajiformes	+	+	−	Continuous and semi-discontinuous (corner tesserae)
G. micrura	Myliobatiformes	+	+	−	Semi-discontinuous (corner tesserae)
Torpedo sp.	Torpediniformes	+	+	−	
R. ancylostoma	Rhinopristiformes	+, t	+, t	−	
P. productus	Rhinopristiformes	+, t	+, t	−	Discontinuous (tessellated)
C. taurus	Lamniformes	+, t	+, t	−	
H. colliei	Chimaeriformes	+, t	−	−	
C. crepidater	Squaliformes	+, t	−	−	Discontinuous (reduced)
E. spinax	Squaliformes	+, t	−	−	

+ indicates that the mineralized tissue is detected, as opposed to −, t indicates that the tissue is located within a tessera, and prox and dist are specified when the tissue is restricted to the proximal (facing the neural tube) and distal (facing muscular attachments) sides of the neural arch, respectively. c, cartilage; pc, perichondrium.

FIGURE 10 | Phylogenetic relationships of the main chondrichthyan groups sampled in this study showing the distribution of neural arch mineralization architecture (silhouettes: green, continuous mineralization; red, semi-discontinuous mineralization; yellow, discontinuous mineralization) and histotypes (F, fibrous mineralization; G, globular mineralization; L, lamellar mineralization). Evolutionary events are located on the tree branches based on reconstructions following a most parsimonious model.

continuously mineralized neural arches in an Heterodontiform, a Squatiniform, most Carcharhiniformes examined in this study, and a Rajiform (**Figure 10**). Fibrous mineralization is also identified in the perichondrial zone of both corner and standard tesserae (**Table 2**). Here we wish to discuss the hypothesis of fibrous mineralization to be naturally mineralizing fibrocartilage, as previously suggested by Ørvig (1951) and Eames et al. (2007). Mineralized fibrocartilages were described in tetrapod entheses that join tendons to bones (Benjamin and Ralphs, 1998) and surrounding rib cartilage (Claassen et al., 1996). Fibrocartilage histology shows strong variation, ranging from almost hyaline to highly fibrous (similar to tendons) in mammals (Wachsmuth et al., 2006) and bony fishes (Benjamin, 1990). Similar variation is observed in our sample, where fibrous mineralization resembles more hyaline-type cartilage crossed by fibers in *P. glauca* (**Figures 8K,L**). This hypothesis would also explain the presence of type II collagen and a thin layer identified as "supra-tesseral cartilage" in the perichondrial surface of tesserae in some species (Seidel et al., 2017). Further histochemical, histological, and cellular characterization is therefore needed to better define the nature of this tissue and compare it to tetrapod tissues.

Beyond the nature of this tissue, we show that perichondrial fibrous mineralization is widely present in skeletal tissues of elasmobranchs. Ancestral character state reconstruction by a most-parsimonious model (**Supplementary Material 1** and summarized in **Figure 10**) suggests that this histotype is ancestral to elasmobranchs (as previously hypothesized by Atake et al., 2019). This scenario implies a secondary loss of fibrous mineralization in *C. crepidater* and *E. spinax*. Considering the secondary loss of mineralization observed in extant holocephalans (Maisey et al., 2020; Pears et al., 2020), it is also plausible that fibrous mineralization is ancestral to all chondrichthyans but lost in holocephalans. Fibrous mineralization may then be a remnant of forms of mineralization found in early vertebrates. As a consequence, a review of the paleontological data is needed, especially in stem gnathostomes and agnathan taxa where several forms of perichondrial bone (cellular or acellular, as described in placoderm taxa Ørvig, 1951 or galeaspid and osteostracan taxa, as reviewed by Donoghue and Sansom, 2002) may be revised in light of this fibrous mineralization that covers cartilaginous skeletal units. Further comparison with extant and extinct taxa of bony fishes may also uncover similar tissues outside of chondrichthyans. Only this information may shed light on the evolution of fibrous mineralization and its significance to the evolution of a mineralized skeleton in vertebrates.

4.3.2. Lamellar Mineralization and Putative Bone in Cartilaginous Fishes

The continuous architecture always includes fibrous mineralization in the distal part of the neural arch but we identified lamellar, instead of fibrous, mineralization in the proximal side of the neural arch of two galeomorph species (**Table 2**). The fibrous and lamellar mineralizations histologically differ in that the former contains numerous cells, as opposed to the latter where only very few cells are observed, and by the arrangement of fibers. Another difference is the lack

of a thick unmineralized connective tissue surrounding the lamellar mineralization (see **Figure 2C'**, as opposed to the situation in other galeomorphs, see **Figures 9G',K'**). Bone-like tissue was previously reported in the neural arches of Carcharhiniformes (Peignoux-Deville et al., 1982; Eames et al., 2007) and Rajiformes (Atake et al., 2019). These previous studies did not distinguish the cellular from almost acellular tissues and the histological staining results in the work of Atake et al. (2019) better support the presence of fibrous mineralization in both the proximal and distal sides of the neural arches of *L. erinacea* and *B. eatonii*. As a consequence, the lamellar mineralized pattern as defined in our work has only been described so far in *S. canicula* and most probably in *C. ventriosum* (Eames et al., 2007) (both Carcharhiniformes), and in *C. punctatum* (Orectolobiformes). Considering these results, ancestral character state reconstruction with a most-parsimonious model suggests parallel evolution of this lamellar pattern in Carcharhiniformes and Orectolobiformes (**Supplementary Material 2**, summarized in **Figure 10**). Still, our observations and hypothesis need to be confirmed with broader sampling among Orectolobiform species, including older specimens. As a broader conclusion, our results support a recent evolution of this trait, making it unlikely to be homologous to any bone type found in early vertebrates.

4.4. Concluding Remarks

Tessellated cartilage is considered a synapomorphy of chondrichthyans (reviewed in Maisey, 2013) and displays a high variety of tessera morphologies and spatial arrangements (Summers et al., 1998; Seidel et al., 2016; Maisey et al., 2020; Pears et al., 2020). What could be considered classical, polygonal and flat tesserae as described in extant batoids are assumed to be the ancestral morphology of chondrichthyan tesserae and to have further undergone size and shape alterations during the evolution of different groups, including strong size regression as found in holocephalans (Pears et al., 2020). Here we have described other mineralization architectures in elasmobranchs, where cartilage surfaces can be continuously mineralized or covered by a combination of tesserae and larger mineralized elements. The reconstruction of an ancestral state for the architecture character under maximum parsimony only suggests that mineralization of the neural arches was ancestrally continuous in selachians, considering a secondary reduction of mineralization in our sampled Lamniform (**Supplementary Material 3**). More samples are necessary to generate hypotheses on chondrichthyans and elasmobranchs.

Besides, we never observed any complete absence of mineralization in our samples. What could be considered a minimal state of mineralization was located in a subperichondrial zone of the hyaline cartilaginous matrix of neural arches (in *H. colliei*, *E. spinax*, and *C. crepidater*). This zone was previously considered as the initiator for further mineralization that would propagate from the hyaline cartilage toward the perichondrium (Ørvig, 1951). It is plausible that the process and pattern of tissue mineralization in elasmobranchs (microscale analysis) might be completely independent of the process of architecture regulation (mesoscale analysis) that has led to

the derived evolution of tesserae in chondrichthyans. As a consequence, if mineralized tissues are comparable in continuous and discontinuous mineralized architectures, evolution between these two states may simply entail a variation in the intensity of one regulatory signal (as suggested by Maisey et al., 2020) that would constrain the size of the mineralized elements, from tesserae as minimal objects to fully mineralized structures, with intermediate states involving the massive elements described in some neural arches of batoids.

Finally, the occurrence of a reduced tessellated pattern in phylogenetically distant groups (Squaliformes and holocephalans) questions the existence of ecological signals able to drive such convergent evolution. Deep-water shark species are known to display reduced mineralization of the endoskeleton as compared to shallower species (Dean et al., 2015; Seidel et al., 2016). *H. colliei* is not restricted to deep water habitats (Barnett et al., 2012) but holocephalans are characterized by a reduction of mineralized structures (Pears et al., 2020) and are the chondrichthyan group found in deepest waters (Priede and Froese, 2013). As a conclusion, ecological constraints, such as deep-water habitat may have convergently driven loss of mineralization in chondrichthyans. It is assumed that such a reduced amount of mineralization could contribute to energetic trade-offs by impacting buoyancy and metabolic costs of locomotion (Blaxter et al., 1971; Blaxter, 1980), however, more data on chondrichthyans are needed to challenge this hypothesis.

DATA AVAILABILITY STATEMENT

The original contributions presented in the study are included in the article/**Supplementary Material**, further inquiries can be directed to the corresponding author/s.

ETHICS STATEMENT

Ethical review and approval was not required for the animal study because no handling of live specimens was necessary for this study.

AUTHOR CONTRIBUTIONS

FB and MD-T designed the experimental setup, prepared the samples, imaged and analyzed the results, and drafted the manuscript. SE, MB, and NP performed the histological sections and staining. FAL-R collected the samples. All authors agree to be accountable for the content of the work.

FUNDING

ACKNOWLEDGMENTS

SUPPLEMENTARY MATERIAL

The Supplementary Material for this article can be found online at: https://www.frontiersin.org/articles/10.3389/fevo. 2021.660767/full#supplementary-material

REFERENCES

Applegate, S. (1967). "A survey of shark hard parts," in *Sharks, Skates and Rays*, eds P. Gilbert, R. Mathewson, and D. Rall (Baltimore, MD: The Johns Hopkins Press), 37–67.

Atake, O. J., Cooper, D. M. L., and Eames, B. F. (2019). Bone-like features in skate suggest a novel elasmobranch synapomorphy and deep homology of trabecular mineralization patterns. *Acta Biomater.* 84, 424–436. doi: 10.1016/j.actbio.2018.11.047

Barnett, L. A., Earley, R. L., Ebert, D. A., and Cailliet, G. M. (2009). Maturity, fecundity, and reproductive cycle of the spotted ratfish, *Hydrolagus colliei. Mar. Biol.* 156, 301–316. doi: 10.1007/s00227-008-1084-y

Barnett, L. A. K., Ebert, D. A., and Cailliet, G. M. (2012). Evidence of stability in a chondrichthyan population: case study of the spotted ratfish *Hydrolagus colliei* (Chondrichthyes: Chimaeridae). *J. Fish Biol.* 80, 1765–1788. doi: 10.1111/j.1095-8649.2011.03216.x

Bejarano-Álvarez, M., Galván-Magaña, F., and Ochoa-Báez, R. I. (2011). Reproductive biology of the scalloped hammerhead shark *Sphyrna lewini*

(Chondrichthyes: Sphyrnidae) off southwest Mexico. *Aqua Int. J. Ichthyol.* 17, 11–22.

Benjamin, M. (1990). The cranial cartilages of teleosts and their classification. *J. Anat.* 169, 153–172.

Benjamin, M., and Ralphs, J. R. (1998). Fibrocartilage in tendons and ligaments–an adaptation to compressive load. *J. Anat.* 193, 481–494. doi: 10.1046/j.1469-7580.1998.19340481.x

Blaxter, J. H. S. (1980). "The effect of hydrostatic pressure on fishes," in *Environmental Physiology of Fishes. NATO Advanced Study Institutes Series (Series A: Life Science)*, Vol. 35, ed M. A. Ali (Boston, MA: Springer). doi: 10.1007/978-1-4899-3659-2_13

Blaxter, J. H. S., Wardle, C. S., and Roberts, B. L. (1971). Aspects of the circulatory physiology and muscle systems of deep-sea fish. *J. Mar. Biol. Assoc.* 51, 991–1006. doi: 10.1017/S0025315400018105

Bustamante, C., and Bennett, M. B. (2013). Insights into the reproductive biology and fisheries of two commercially exploited species, shortfin mako (*Isurus oxyrinchus*) and blue shark (*Prionace glauca*), in the southeast Pacific Ocean. *Fish. Res.* 143, 174–183. doi: 10.1016/j.fishres.2013.02.007

Capapé, C., Guélorget, O., Siau, Y., Vergne, Y., and Quignard, J. P. (2007). Reproductive biology of the thornback ray *Raja clavata* (Chondrichthyes: Rajidae) from the coast of Languedoc (southern France, northern Mediterranean). *Vie Milieu* 57, 83–90.

Capapé, C., Reynaud, C., Vergne, Y., and Quignard, J. P. (2008). Biological observations on the smallspotted catshark *Scyliorhinus canicula* (Chondrichthyes: Scyliorhinidae) off the Languedocian coast (southern France, northern Mediterranean). *Pan Am. J. Aquat. Sci.* 3, 282–289.

Chaumel, J., Schotte, M., Bizzarro, J. J., Zaslansky, P., Fratzl, P., Baum, D., et al. (2020). Co-aligned chondrocytes: zonal morphological variation and structured arrangement of cell lacunae in tessellated cartilage. *Bone* 134:115264. doi: 10.1016/j.bone.2020.115264

Claassen, H., Kampen, W. U., and Kirsch, T. (1996). Localization of collagens and alkaline phosphatase activity during mineralization and ossification of human first rib cartilage. *Histochem. Cell Biol.* 105, 213–219. doi: 10.1007/BF01462294

Compagno, L. J. V. (1984). Sharks of the world: an annotated and illustrated catalogue of shark species known to date. *FAO Species Catalog. Fish. Purposes* 2, 175–176.

Criswell, K. E., Coates, M. I., and Gillis, J. A. (2017). Embryonic development of the axial column in the little skate, *Leucoraja erinacea*. *J. Morphol.* 278, 300–320. doi: 10.1002/jmor.20637

Dean, M. N., Ekstrom, L., Monsonego-Ornan, E., Ballantyne, J., Witten, P. E., Riley, C., et al. (2015). Mineral homeostasis and regulation of mineralization processes in the skeletons of sharks, rays and relatives (Elasmobranchii). *Semin. Cell Dev. Biol.* 46, 51–67. doi: 10.1016/j.semcdb.2015.10.022

Dean, M. N., Mull, C. G., Gorb, S. N., and Summers, A. P. (2009). Ontogeny of the tessellated skeleton: insight from the skeletal growth of the round stingray *Urobatis halleri*. *J. Anat.* 215, 227–239. doi: 10.1111/j.1469-7580.2009.01116.x

Dean, M. N., and Summers, A. P. (2006). Mineralized cartilage in the skeleton of chondrichthyan fishes. *Zoology* 109, 164–168. doi: 10.1016/j.zool.2006.03.002

Debiais-Thibaud, M. (2019). "The evolution of endoskeletal mineralisation in chondrichthyan fish," in *Evolution and Development of Fishes, Chapter 6*, eds Z. Johanson, C. Underwood, and M. Richter (Cambridge: Cambridge University Press), 110–125. doi: 10.1017/9781316832172.007

Debiais-Thibaud, M., Simion, P., Ventéo, S., Muñoz, D., Marcellini, S., Mazan, S., et al. (2019). Skeletal mineralization in association with type x collagen expression is an ancestral feature for jawed vertebrates. *Mol. Biol. Evol.* 36, 2265–2276. doi: 10.1093/molbev/msz145

Donoghue, P. C. J., and Sansom, I. J. (2002). Origin and early evolution of vertebrate skeletonization. *Microsc. Res. Tech.* 59, 352–372. doi: 10.1002/jemt.10217

Eames, B. F., Allen, N., Young, J., Kaplan, A., Helms, J. A., and Schneider, R. A. (2007). Skeletogenesis in the swell shark *Cephaloscyllium ventriosum*. *J. Anat.* 210, 542–554. doi: 10.1111/j.1469-7580.2007.00723.x

Ebert, D. A., Fowler, S., and Compagno, L. J. V. (2013). *Sharks of the World: A Fully Illustrated Guide*. Plymouth: Wild Nature Press.

Enault, S., Adnet, S., and Debiais-Thibaud, M. (2016). Skeletogenesis during the late embryonic development of the catshark *Scyliorhinus canicula* (Chondrichthyes; Neoselachii). *MorphoMuseuM* 1:e2. doi: 10.18563/m3.1.4.e2

Enault, S., Muñoz, D. N., Silva, W. T. A. F., Borday-birraux, V., Bonade, M., Oulion, S., et al. (2015). Molecular footprinting of skeletal tissues in the catshark Scyliorhinus canicula and the clawed frog *Xenopus tropicalis* identifies conserved and derived features of vertebrate calcification. *Front. Genet.* 6:283. doi: 10.3389/fgene.2015.00283

Finarelli, J. A., and Coates, M. I. (2014). Chondrenchelys problematica (Traquair 1888) redescribed: a Lower Carboniferous, eel-like holocephalan from Scotland. *Earth Environ. Sci. Trans. R. Soc. Edinb.* 105, 35–59. doi: 10.1017/S1755691014000139

Goodrich, E. S. (1930). *Studies on the Structure & Development of Vertebrates*. London: Macmillan and Co.

Hall, B. K. (2015). *Bones and Cartilage, 2nd Edn.* Oxford: Elsevier-Academic Press.

Hall, B. K., and Witten, P. E. (2019). "Plasticity and variation of skeletal cells and tissues and the evolutionary development of actinopterygian fishes," in *Evolution and Development of Fishes, Chapter 7*, eds Z. Johanson, C. Underwood, and M. Richter (Cambridge: Cambridge Université Press), 126–143. doi: 10.1017/9781316832172.008

Hasse, C. (1879). *Das natürliche System der Elasmobranchier auf Grundlage des Baues und der Entwicklung ihrer Wirbelsäule*, Vol. I Allgemei. Jena: Eine morphologische und paläontologische Studie.

Hilton, M. J., Tu, X., Cook, J., Hu, H., and Long, F. (2005). Ihh controls cartilage development by antagonizing Gli3, but requires additional effectors to regulate osteoblast and vascular development. *Development* 132, 4339–4351. doi: 10.1242/dev.02025

Johanson, Z., Boisvert, C. A., Maksimenko, A., Currie, P., and Trinajstic, K. (2015). Development of the synarcual in the elephant sharks (Holocephali; Chondrichthyes): implications for vertebral formation and fusion. *PLoS ONE* 10:e0135138. doi: 10.1371/journal.pone.0135138

Kemp, N. E., and Westrin, S. K. (1979). Ultrastructure of calcified cartilage in the endoskeletal tesserae of sharks. *J. Morphol.* 160, 75–109. doi: 10.1002/jmor.1051600106

Last, P., Naylor, G., Séret, B., White, W., de Carvalho, M., and Stehmann, M. (2016). *Rays of the World*. Clayton South, VIC: CSIRO Publishing.

Leurs, N., Martinand-Mari, C., Vento, S., Haitina, T., and Debiais-Thibaud, M. (2021). Evolution of matrix gla and bone gla protein genes in jawed vertebrates. *Front. Genet.* 12:245. doi: 10.3389/fgene.2021.620659

Licht, M., Schmuecker, K., Huelsken, T., Hanel, R., Bartsch, P., and Paeckert, M. (2012). Contribution to the molecular phylogenetic analysis of extant holocephalan fishes (Holocephali, Chimaeriformes). *Organ. Divers. Evol.* 12, 421–432. doi: 10.1007/s13127-011-0071-1

Lucifora, L. O., Menni, R. C., and Escalante, A. H. (2002). Reproductive ecology and abundance of the sand tiger shark, *Carcharias taurus*, from the southwestern Atlantic. *ICES J. Mar. Sci.* 59, 553–561. doi: 10.1006/jmsc.2002.1183

Lucifora, L. O., Menni, R. C., and Escalante, A. H. (2004). Reproductive biology of the school shark, *Galeorhinus galeus*, off Argentina: support for a single south western Atlantic population with synchronized migratory movements. *Environ. Biol. Fishes* 71, 199–209. doi: 10.1007/s10641-004-0305-6

Maddison, W. P., and Maddison, D. R. (2019). *Mesquite: A Modular System for Evolutionary Analysis*. Available online at: http://www.mesquiteproject.org

Maisey, J. G. (2013). The diversity of tessellated calcification in modern and extinct chondrichthyans. *Rev. Paléobiol.* 32, 355–371.

Maisey, J. G., Denton, J. S. S., Burrow, C., and Pradel, A. (2020). Architectural and ultrastructural features of tessellated calcified cartilage in modern and extinct chondrichthyan fishes. *J. Fish Biol.* 98, 919–941. doi: 10.1111/jfb.14376

Márquez-Farías, J. F. (2007). Reproductive biology of shovelnose guitarfish Rhinobatos productus from the eastern Gulf of California México. *Mar. Biol.* 151, 1445–1454. doi: 10.1007/s00227-006-0599-3

Mayoral, E. E., Schultz, R., Rosemberg, S., Suzuki, L., Nunes de Oliveira, L. A., and Kay, F. U. (2014). Thanatophoric dysplasia : case report of an autopsy complemented by postmortem computed tomographic study. *Autopsy Case Rep.* 4, 35–41. doi: 10.4322/acr.2014.019

Meese, E. N., and Lowe, C. G. (2020). Environmental effects on daytime sheltering behaviors of California horn sharks (*Heterodontus francisci*). *Environ. Biol. Fishes* 103, 703–717. doi: 10.1007/s10641-020-00977-6

Moore, D. M., Neat, F. C., and McCarthy, I. D. (2013). Population biology and ageing of the deep water sharks *Galeus melastomus*, *Centroselachus crepidater* and *Apristurus aphyodes* from the Rockall Trough, north-east Atlantic. *J. Mar. Biol. Assoc.* 93, 1941–1950. doi: 10.1017/S0025315413000374

Naylor, G. J. P., Caira, J. N., Jensen, K., Rosana, K. A. M., Straube, N., and Lakner, C. (2012). "Elasmobranch phylogeny: a mitochondrial estimate based on 595 species," in *Biology of Sharks and Their Relatives, Chapter 2, 2nd Edn.*, eds J. C. Carrier, J. A. Musick, and M. R. Heithaus (Boca Raton, FL: CRC Press), 31–56. doi: 10.1201/b11867-4

Ørvig, T. (1951). Histologic studies of Placoderms and fossil Elasmobranchs. I: the endoskeleton, with remarks on the hard tissues of lower vertebrates in general. *Arkiv Zool.* 2:322.

Pears, J., Johanson, Z., Trinajstic, K., Dean, M. N., and Boisvert, C. A. (2020). Mineralization of the callorhinchus vertebral column (Holocephali; Chondrichthyes). *Front. Genet.* 11:1477. doi: 10.3389/fgene.2020.571694

Peignoux-Deville, J., Lallier, F., and Vidal, B. (1982). Evidence for the presence of osseous tissue in dogfish vertebrae. *Cell Tissue Res.* 222, 605–614. doi: 10.1007/BF00213858

Porcu, C., Marongiu, M. F., Follesa, M. C., Bellodi, A., Mulas, A., Pesci, P., et al. (2014). Reproductive aspects of the velvet belly *Etmopterus spinax*

(Chondrichthyes: Etmopteridae), from the central western Mediterranean Sea. Notes on gametogenesis and oviducal gland microstructure. *Mediterr. Mar. Sci.* 15, 313–326. doi: 10.12681/mms.559

Priede, I. G., and Froese, R. (2013). Colonization of the deep sea by fishes. *J. Fish Biol.* 83, 1528–1550. doi: 10.1111/jfb.12265

Ridewood, W. G., and MacBride, E. W. (1921). VIII. On the calcification of the vertebral centra in sharks and rays. *Philos. Trans. R. Soc. Lond. B* 210, 311–407. doi: 10.1098/rstb.1921.0008

Romero-Caicedo, A. F., Galván-Magaña, F., Hernández-Herrera, A., and Carrera-Fernández, M. (2016). Reproductive parameters of the Pacific angel shark *Squatina californica* (Selachii: Squatinidae). *J. Fish Biol.* 88, 1430–1440. doi: 10.1111/jfb.12920

Ryll, B., Sanchez, S., Haitina, T., Tafforeau, P., and Ahlberg, P. E. (2014). The genome of Callorhinchus and the fossil record: a new perspective on scpp gene evolution in gnathostomes. *Evol. Dev.* 16, 123–124. doi: 10.1111/ede.12071

Seidel, R., Blumer, M., Chaumel, J., Amini, S., and Dean, M. N. (2020). Endoskeletal mineralization in chimaera and a comparative guide to tessellated cartilage in chondrichthyan fishes (sharks, rays and chimaera). *J. R. Soc. Interface* 17:20200474. doi: 10.1098/rsif.2020.0474

Seidel, R., Blumer, M., Pechriggl, E.-J., Lyons, K., Hall, B. K., Fratzl, P., et al. (2017). Calcified cartilage or bone? Collagens in the tessellated endoskeletons of cartilaginous fish (sharks and rays). *J. Struct. Biol.* 200, 54–71. doi: 10.1016/j.jsb.2017.09.005

Seidel, R., Lyons, K., Blumer, M., Zaslansky, P., Fratzl, P., Weaver, J. C., et al. (2016). Ultrastructural and developmental features of the tessellated endoskeleton of elasmobranchs (sharks and rays). *J. Anat.* 229, 681–702. doi: 10.1111/joa.12508

Smith, M. M., Underwood, C., Goral, T., Healy, C., and Johanson, Z. (2019). Growth and mineralogy in dental plates of the holocephalan *Harriotta raleighana* (Chondrichthyes): novel dentine and conserved patterning combine to create a unique chondrichthyan dentition. *Zool. Lett.* 5, 1–30. doi: 10.1186/s40851-019-0125-3

Summers, A. P., Koob, T. J., and Brainerd, E. L. (1998). Stingray jaws strut their stuff. *Nature* 395, 450–451. doi: 10.1038/26649

Tarazona, O. A., Slota, L. A., Lopez, D. H., Zhang, G., and Cohn, M. J. (2016). The genetic program for cartilage development has deep homology within Bilateria. *Nature* 533, 86–89. doi: 10.1038/nature17398

Wachsmuth, L., Söder, S., Fan, Z., Finger, F., and Aigner, T. (2006). Immunolocalization of matrix proteins in different human cartilage subtypes. *Histol. Histopathol.* 21, 477–485. doi: 10.14670/HH-21.477

Whiteman, P. (1973). The quantitative measurement of Alcian Blue-glycosaminoglycan complexes. *Biochem. J.* 131, 343–350. doi: 10.1042/bj1310343

Witten, P. E., and Huysseune, A. (2009). A comparative view on mechanisms and functions of skeletal remodelling in teleost fish, with special emphasis on osteoclasts and their function. *Biol. Rev. Camb. Philos. Soc.* 84, 315–346. doi: 10.1111/j.1469-185X.2009.00077.x

Witten, P. E., Huysseune, A., and Hall, B. K. (2010). A practical approach for the identification of the many cartilaginous tissues in teleost fish. *J. Appl. Ichthyol.* 26, 257–262. doi: 10.1111/j.1439-0426.2010.01416.x

Xiong, H., Rabie, A. B. M., and Hagg, U. (2005). Mechanical strain leads to condylar growth in adult rats. *Front. Biosci.* 10, 65–73. doi: 10.2741/1507

Yokota, L., Goitein, R., Gianeti, M. D., and Lessa, R. T. (2012). Reproductive biology of the smooth butterfly ray *Gymnura micrura*. *J. Fish Biol.* 81, 1315–1326. doi: 10.1111/j.1095-8649.2012.03413.x

Zhang, G., and Cohn, M. J. (2006). Hagfish and lancelet fibrillar collagens reveal that type II collagen-based cartilage evolved in stem vertebrates. *Proc. Natl. Acad. Sci. U.S.A.* 103, 16829–16833. doi: 10.1073/pnas.0605630103